Petroleum Geoscience

Estimation of net apparent erosion in the southwestern Barents Sea by applying velocity inversion analysis

--Manuscript Draft--

Manuscript Number:	petgeo2018-002R3
Article Type:	Research article
Full Title:	Estimation of net apparent erosion in the southwestern Barents Sea by applying velocity inversion analysis
Short Title:	Net apparent erosion in the SW Barents Sea
Corresponding Author:	Dimitrios Ktenas Universitetet i Tromso matematisk-naturvitenskapelige fakultet Tromsø, Troms NORWAY
Corresponding Author E-Mail:	dimitriosktenas@gmail.com
Other Authors:	Ivar Meisingset
	Erik Henriksen
	Jesper Kresten Nielsen
Abstract:	The southwestern Barents Sea was subject to significant uplift and erosion during the Cenozoic, processes which are believed to have had a significant impact on hydrocarbon maturation and migration in the area. The current study uses compaction of shale- and sand-dominated layers to make a map of net apparent erosion throughout the southwestern Barents Sea. The map shows regional trends consistent with deep-seated isostatic uplift of the crust in combination with glacial erosion as a driving mechanism for the erosion. We find increased erosion towards the north and decreased erosion towards the west, in the western Barents Sea. The trend of highest erosion has an axis stretching in a southeast to northwest orientation towards Svalbard. This indicates a major change in the crustal uplift pattern in the transition from the Norwegian mainland to the Barents Sea. The velocity inversion method used in this study combined with a two-baseline normal compaction trend model demonstrates a reliable procedure for accurate erosion estimations. It allows erosion estimates from layers with different lithologies to be integrated into a common interpretation and differences to be interpreted geologically, for example, an apparent facies change to a mixed sand-shale lithology, possibly with reservoir quality sands developed, in the Cretaceous on the Bjarmeland Platform.
Manuscript Classifications:	Basin analysis; Exploration case studies; Geophysics
Additional Information:	
Question	**Response**
Are there any conflicting interests, financial or otherwise?	No
Samples used for data or illustrations in this article have been collected in a responsible manner	Confirmed
Response to Reviewers:	Please find attached the .doc file 'Response to reviewer'.

Estimation of net apparent erosion in the southwestern Barents Sea by applying velocity inversion analysis

Dimitrios Ktenas[1]*, Ivar Meisingset[2], Erik Henriksen[1,3], Jesper Kresten Nielsen[4]

[1] Research Centre for Arctic Petroleum Exploration (ARCEx), Department of Geosciences, University of Tromsø - The Arctic University of Norway, Dramsveien 201, NO-9037 Tromsø, Norway

[2] ModelGeo AS, Borgenbanken 5, NO-0370 Oslo, Norway

[3] Henriksen Maritime Consultancy AS, Los Holtes vei 49, NO-9414 Harstad, Norway

[4] MOL Norge AS, Trelastgata 3, NO-0191 Oslo, Norway

*Corresponding author. E-mail: dimitriosktenas@gmail.com

Keywords: Velocity inversion, Normal Compaction Trend (NCT), Net apparent erosion, Maximum burial, Shale compaction, Southwestern Barents Sea

Abstract

The southwestern Barents Sea was subject to significant uplift and erosion during the Cenozoic, processes which are believed to have had a significant impact on hydrocarbon maturation and migration in the area. The current study uses compaction of shale- and sand-dominated layers to make a map of net apparent erosion throughout the southwestern Barents Sea. The map shows regional trends consistent with deep-seated isostatic uplift of the crust in combination with glacial erosion as a driving mechanism for the erosion. We find increased erosion towards the north and decreased erosion towards the west, in the western Barents Sea. The trend of highest erosion has an axis stretching in a southeast to northwest orientation towards Svalbard. This

indicates a major change in the crustal uplift pattern in the transition from the Norwegian mainland to the Barents Sea. The velocity inversion method used in this study combined with a two-baseline normal compaction trend model demonstrates a reliable procedure for accurate erosion estimations. It allows erosion estimates from layers with different lithologies to be integrated into a common interpretation and differences to be interpreted geologically, for example, an apparent facies change to a mixed sand-shale lithology, possibly with reservoir quality sands developed, in the Cretaceous on the Bjarmeland Platform.

Introduction

The southwestern Barents Sea (Fig. 1) has undergone a series of regional uplift and erosion episodes during the Mesozoic and Cenozoic, where the late Cenozoic episodes appear to be the most important. Due to the large hiatus in the rock record there are many alternative proposals for the amount, timing and magnitude of the erosion events (Vorren et al. 1991; Faleide et al. 1996; Dimakis et al. 1998; Cavanagh et al. 2006; Green & Duddy 2010; Henriksen et al. 2011a; Laberg et al. 2012; Duran et al. 2013; Zieba et al. 2014; Baig et al. 2016; Zattin et al. 2016; Ktenas et al. 2017). This leaves a great deal of uncertainty with respect to the geological history of the southwestern Barents Sea, with consequences for hydrocarbon exploration. Rapid erosion and differential uplift and tilting of the study area has led to leakage of hydrocarbons from pre-existing traps, the phase transition from oil to gas, gas expansion, seal failure and cooling of source rocks (Doré & Jensen 1996; Henriksen et al. 2011a). For the known hydrocarbon accumulations, these effects are still not fully understood. Therefore much effort has been put into the task of quantifying the amounts of uplift and erosion in the Barents Sea.

The aim of this study is to investigate net apparent erosion in the southwestern Barents Sea, defined as the difference between the maximum and the present-day burial depths for a specified horizon (Henriksen et al. 2011a), and to determine the regional variation and magnitude of the erosion by studying the compaction of selected layers. Compaction based net apparent erosion estimates depend on a small number of model assumptions and can therefore give accurate and reliable results over large areas. This is valid, as long as the normal compaction trends used are appropriate, and geological factors apart from burial which influence the velocity of a layer are not misinterpreted as erosion (Anell et al. 2009). The method used in this study is a multi-layer velocity inversion, which in the context of the study means inversion of velocity data to geological parameters by means of a Normal Compaction Trend (NCT) model with baselines for more than one type of lithology. Velocity inversion is a rock physics method which solves simultaneously for porosity (Schlumberger Limited, 2009), pseudo-lithology (Peikert 1985; Hubred & Meisingset 2013), pore pressure (Mukerji et al. 2002; Johansen et al. 2015; Meisingset et al. 2017) and net apparent erosion (Gateman & Avseth 2016; Johansen 2016; Ktenas et al. 2017). Ktenas et al. (2017) developed a velocity inversion NCT model referred to as the 'Dikte NCT' for use with sonic logs in the southwestern Barents Sea wells. This model has two baselines, for Cretaceous shale and Lower Jurassic–Upper Triassic sandstone dominated layers. In this study the Dikte NCT model is utilised on interpreted seismic profiles and time maps. These are depth converted with a check-shot calibrated high-quality regional velocity model.

The multi-layer velocity inversion method allows net apparent erosion to be estimated in layers with different lithologies in the same geographical location. Inversion of interpreted profiles with many layers, where the results can be compared with the seismic data, allows investigation of which layers are most useful for net apparent erosion estimation. Artefacts caused by high velocity contrast boundaries such as the edges of structural highs and tops of carbonate layers, and layers where the erosion estimates fail (due to lithofacies changes, overpressure and insufficient layer thickness) can be studied in detail. Velocity inversion of regional maps provides full coverage of the study area. When the methods are combined, it is possible to select optimal layers from the map sets in each geographical location, and combine them in order to make a best case net apparent erosion map.

Net apparent erosion estimates by velocity inversion of profiles and maps have one important limitation: they rely on the assumption that the layer has a uniform lithology and the applied baseline is appropriate for the whole layer. In contrast, this is not a requirement for velocity inversion of wells (using sonic logs) where the lithology variation can be handled by aligning the baseline with the part of the log curve which has the correct lithology. Therefore, while the regional variation (shape) of net apparent erosion is best estimated from maps, the magnitude of erosion estimates from wells will be more accurate. Furthermore, the best overall result is obtained when well and map (and profile) results are integrated.

Geological setting

The study area is located in the southwestern Barents Shelf (Fig. 1), a region with a geological evolution that dates back to the Paleozoic and further developed during the Mesozoic and Cenozoic with the opening of the Norwegian-Greenland Sea and Eurasia basin (Faleide et al. 1993; 2008; Tsikalas et al. 2012). The Barents Shelf is represented by a shallow platform which has experienced several episodes of periodic rifting, uplift and erosion, tilting and folding (Fig. 2) (Faleide et al. 1993; 2008). These processes have contributed to the present-day tectonic configuration of the southwestern Barents Sea and the structural framework is dominated by key features such as sub-platforms, highs and basins (Fig. 1) (Rønnevik & Jacobsen 1984; Gabrielsen et al. 1990; Faleide et al. 2008; Henriksen et al. 2011b). The geological evolution and tectonostratigraphy of the southwestern Barents Sea has been documented in detail by Faleide et al. (2008) and Henriksen et al. (2011b) and references therein (Fig. 2).

During the late Cenozoic, the southwestern Barents Sea underwent episodes of broad uplift and erosion. Due to limited stratigraphic control, the exact timing and number of episodes is poorly constrained. A simplification which is useful for basin modelling is to assume two episodes: one which pre-dates the Pleistocene sediments (e.g. Duran et al. 2013; Lasabuda et al. 2018) present in the area (and for basin modelling purposes can be assumed to have created a flat surface), and one which post-dates (e.g. Cavanagh et al. 2006; Nielsen et al. 2015) these sediments (and for basin modelling purposes can be assumed to be responsible for the present-day seabed terrain).

There is abundant literature on proposed mechanisms of uplift and erosion in the Fennoscandian-Barents Sea, based on: deep-seated thermal anomalies (Dimakis et al. 1998), mantle flow phase changes (Riis & Fjeldskaar 1992), isostatic response and sedimentary unloading (Riis & Fjeldskaar 1992), glacial erosion due to isostatic compensation (Eidvin et al. 1993), flexural response to sediment loading and intra-plate stress (see extensive review by Anell et al. 2009), as well as regional tectonic uplift (Vågnes & Amundsen 1993) related to a North Atlantic gravity anomaly (Cochran & Talwany 1978). The broad regional shape of the southwestern Barents Sea uplift and erosion, is consistent with a regional, isostatic uplift mechanism. Some proposed mechanisms for isostatic uplift include a temperature increase in the mantle (Cochran & Talwany 1978), and/or chemical alteration of the base of the lithosphere, creating less dense minerals such as serpentine (Vågnes & Amundsen 1993).

Zattin et al. (2016), using apatite (U-Th)/He thermochronology data, propose a late Miocene to early Pliocene age for the last important phase of exhumation. They note that while their method does not detect the younger (glacial) exhumation episode during the last 2 million years, it shows that the erosion magnitude of this episode must have been significantly lower than for the older episode. These results are compatible with a regional isostatic uplift mechanism for the older erosion episode along with glacial erosion with associated isostatic rebound for the younger erosion episode. A number of other authors propose different ages of uplift and erosion for the older episode (e.g. Anell et al. 2009 and references therein).

Considering the size of the eroded area and the depth of erosion it is likely that the older episode would have taken a considerable amount of time, and erosion may not have been ceased everywhere in the southwestern Barents Sea until the earliest Pleistocene, when erosion by glacial ice-streams was initiated (Andreassen & Winsborrow 2009; Knies et al. 2009; Bellwald et al. 2018).

Database and Methods

Interpreted seismic horizons, NCT model and velocity model

In this study, 2D regional seismic Profiles A-A’, B-B’ and C-C’ were carefully selected from among the dense 2D and 3D seismic data covering the southwestern Barents Sea (Fig. 1). Well-log data and formation tops from wells on and close to the profiles were calibrated to the seismic (well-to-seismic-tie) in order to obtain an accurate seismic interpretation (Fig. 1). The composite 2D seismic lines were obtained from the Norwegian Diskos National Data Repository (DISKOS) database. Regional time interpreted maps on selected horizons were provided by North E&P AS. The Dikte NCT model and the net apparent erosion map derived from sonic logs used in this study are based on an earlier piece of work carried out on the Norwegian Continental Shelf (NCS) (Ktenas et al. 2017). A regional high velocity cube (Barents Sea velocity cube hiQbe™ model, version BS-0615T) with grid dimensions 3000 x 3000 m laterally and 100 ms vertically from 0–12000 ms TWT has been used for depth conversion and velocity inversion of the interpreted seismic profiles and time maps (Meisingset et al. 2018; First Geo 2017). The hiQbe™ is a commercially available high quality regional velocity model based on seismic processing velocities and check-shots from the public domain and other sources.

Velocity inversion analysis

The use of seismic velocities combined with shale compaction and rock physics for estimation of uplift and erosion is an established exploration geophysics technique and has been used by several workers on the NCS (e.g. Richardsen et al. 1993; Dræge et al. 2014; Baig et al. 2016; Gateman & Avseth 2016). The shale compaction method depends on an NCT baseline for each lithology under study, which defines the increase of velocity with depth. Several compaction trends based on well log data have been published, such as the NCT model for shale and sandstone in the UK-Danish North Sea by Japsen (2000; 2018) and Japsen et al. (2007), the NCT for the northern North Sea (Sclater & Christie 1980, Storvoll et al. 2005), the Dikte NCT model for the southwestern Barents Sea (Ktenas et al. 2017) and the NCT from the Gulf of Mexico area (based on Gardner et al. 1974).

In this study, the Dikte NCT model which has baselines for two lithologies, was used. The model was established based on a database of 40 sonic logs from wells on the NCS (Ktenas et al. 2017). The Dikte baseline for shale-dominated layers, which has been calibrated for use for the Cretaceous shales (CretShale) in the southwestern Barents Sea, was utilized for the Neogene, Paleogene and Cretaceous stratigraphic intervals in this study. The zero uplift reference for this baseline is the Cretaceous shales in selected Norwegian Sea wells, which are thought to consist of a similar litho-facies type as same age shales in the southwestern Barents Sea. The Dikte baseline for mixed sand-shale lithologies, calibrated for use with the Lower Jurassic–Upper Triassic (LJurTrias) intervals in the southwestern Barents Sea, was utilized for layers of Jurassic and Triassic age in this study. The zero uplift reference for this baseline was the Åre Formation of the Norwegian Sea. The Åre Formation (Rhaetian-Pliensbachian) consists mainly of coastal plain deposits, which formed in a similar depositional environment to deposits of the Lower Jurassic Nordmela and Upper Triassic Fruholmen formations in the Barents Sea (Fig. 2). The Dikte NCT model is suitable for subsiding sedimentary basins where the state of the shale compaction disequilibrium is similar to the Norwegian Sea reference area (Ktenas et al. 2017).

Net apparent erosion is computed from an NCT model by depth-shifting the velocity data (from sonic logs, profiles and/or time grids) down to the point where it intersects the baseline. The applied depth shift, is used as an estimate for the net apparent erosion. This is a standard shale compaction method, which assumes that a porous rock will compact mechanically and/or chemically mainly as a consequence of the maximum vertical effective stress and temperature applied to it, and neither decompact, nor compact further through diagenesis, during uplift and erosion. Furthermore, it is assumed that the maximum vertical effective stress and temperature occurs at the maximum depth of burial, and that a precise relationship exists between compaction and velocity (for a given lithology). Neither of these assumptions will always be true, but the deviations from the assumptions are normally minor, and in most cases they can be ignored.

A conceptual model for the net apparent erosion estimation is shown in Figure 3. Velocity inversion of interpreted horizons is performed on a set of layers, where mid-point depth and interval velocity are used as inversion inputs. When the vertical velocity variation within the layer is linear, then the velocity at the mid-point depth will be identical to the interval velocity. These values are therefore the most representative for the layer, when all that is known is the time and depth to top and base (as is the case when the inputs are surfaces from seismic interpretation). Figure 3a shows two layers with their mid-points indicated in terms of depth and velocity. Layer 1 (green) is a Cretaceous shale, and should be referenced to the Dikte CretShale baseline. Layer 2 (yellow) is an Upper Triassic sand/shale layer which should be referenced to the Dikte LJurTrias baseline. Figure 3b shows the mid-points plotted together with the baselines in a net apparent erosion analysis window. The estimated erosion is equal to the vertical distance in metres between the points and their respective baselines. The arrows show the uplift path of the points from their maximum depth of burial, when they were located on the baselines, to their present depth.

Net apparent erosion estimates by velocity inversion of layer mid-points suffers from some limitations when compared with well-log based estimates. Erosion estimation from a well log is an interpretation where the baseline is subjectively aligned with the part of the well log which has the appropriate lithology. In the layer mid-point velocity inversion method, where the only inputs are time and depth at the top and base of the layer, as the calculation is a mathematical average with no possibility for subjective alignment. The NCT baselines may not be fully appropriate if they have been (as in this study) developed from uncalibrated sonic log velocities and are applied to check-shot calibrated velocities. There is also a potential issue with the curvature of the NCT baseline in thick layers, due to the assumption that velocity increases linearly, inherent in the mid-point method. For these reasons, net apparent erosion estimates from mid-point data, such as profiles and time maps, should not be expected to absolutely match the estimates from wells. It is therefore recommended to calibrate net apparent erosion estimates from velocity inversion of layer mid-point data, against estimates from wells.

Another important pitfall in the southwestern Barents Sea is ‘velocity leakage’. This occurs at high velocity contrast boundaries such as the edges of structural highs and tops of carbonate layers. The velocity data used (a regional high quality velocity model) does not have adequate resolution to capture the exact position of such boundaries; in addition, the seismic horizon interpretation, especially when gridded into time surfaces, may not have been placed precisely at the high contrast boundary in the subsurface. Furthermore, the seismic processing velocities that were used in the velocity model may disagree with the seismic interpretation, with regards to boundary position in a zone of poor seismic data quality. These issues can cause high velocities to erroneously appear in a given layer on the low velocity side of the boundary, for example. In this study we term this phenomenon 'velocity leakage'. It is best to avoid relying on layers which lie directly on a high velocity contrast horizon for net apparent erosion estimates.

Results

Net apparent erosion estimates on seismic profiles in the southwestern Barents Sea

Velocity inversion analysis was carried out on three regional interpreted seismic profiles in the southwestern Barents Sea for the Cretaceous and Lower Jurassic-Triassic sequences (Figs 4, 5 and 6). The purpose of the horizon interpretation was to delineate a set of layers which were suitable for estimation of net apparent erosion using the Dikte NCT model (Ktenas et al. 2017).

Profile A-A'

Profile A-A,' running from the west to the east, is shown in Figure 4. The vertical axis is in depth. Figure 4a is coloured by stratigraphic layer, and shows interpreted horizons and faults. The interpreted horizons, which range in age from the seabed to the basement, illustrate the basin configuration as well as the structural changes from the west to the east in the study area. Figure 4b shows the interval velocity from the regional velocity cube extracted along the plane of the profile. Velocities are stable and follow the layers, with an increase against depth which comes from increased compaction, except for some apparent layering (i.e. velocity anomalies) at around 7000 m depth in the Sørvestsnaget Basin towards the shelf edge (lower left corner of Fig. 4b, Layer 10). The seismic data quality here, and thus the quality of the seismic processing velocities, is poor.

Figure 4c consists of two panels. The upper panel shows the net apparent erosion estimates in colour superimposed on the seismic. Net apparent erosion was estimated from the Neogene (Layers 03-07), Paleogene (Layers 08-09) and Cretaceous (Layer 10) (using the CretShale baseline), and Lower Jurassic–Triassic (Layer 13) (using the LJurTrias baseline). These layers are considered to be valid for the inversion study, except for the Layer 10-Cretaceous where the velocities are poor in the Sørvestsnaget Basin. Wells 7220/8-1, 7222/11-1 and 7124/3-1 are superimposed (Figure 4c, upper panel), with coloured tube displays of net apparent erosion estimates from sonic logs (Ktenas et al. 2017). The lower panel in Figure 4c shows the estimated net apparent erosion from each of the inverted profile layers. Net apparent erosion from the corrected map is included for comparison (discussed in detail below). The graph shows stable erosion estimates in the eastern and central parts of the profile as well as significant uncertainty in the west. Enlarged displays of the eastern, middle and western parts of Profile A-A' are shown in Figures 4d–j. The best layers for net apparent erosion estimation in the eastern and middle parts of the profile are Layers 10-Cretaceous and 13-Triassic (Fig. 4d, e, g, h).

Figure 4f illustrates the interpretation process by which valid layers are selected. It shows the net apparent erosion estimates from all of the interpreted layers in the eastern part of Profile A-A', regardless of whether or not the estimates are considered valid. The inversion used the LJurTrias baseline for Layers 17-Carboniferous up to 12-Jurassic and the CretShale baseline for Layers 11-Cretaceous to 01-Neogene. Layers 17-Carboniferous and 16-Permian are carbonate dominated, and as such the LJurTrias baseline is inappropriate; thus the erosion estimates are invalid. Layer 15-Triassic is of Lower Triassic age; it overlies the Permian carbonates (high velocity contrast boundary) and experiences 'velocity leakage' from below. The estimates in this layer are invalid for two reasons: velocity leakage and the LJurTrias baseline being inappropriate for the Lower Triassic. Similarly, it is also inappropriate for layer 14-Triassic, which is of Middle Triassic age. Layer 13-Triassic is of Upper Triassic age, and the LJurTrias baseline is valid. Layers 12-Jurassic and 11-Cretaceous are thin relative to the vertical resolution of the velocity data, and therefore do not give reliable estimates. Layer 10-Cretaceous is valid, with the CretShale baseline. In the upper section, there is one Paleogene (09-Paleogene) and one Neogene layer (03-Neogene). The Paleogene layer has a sufficient thickness, but the well indicates that it is not well aligned with Layer 10-Cretaceous, and the CretShale baseline is therefore invalid for it here. The Neogene layer is thin and close to the seabed. This interpretation procedure leaves us with two valid layers for net apparent erosion estimation in the eastern part of Profile A-A', namely 10-Cretaceous and 13-Triassic.

On the eastern part of the Profile A-A', on the Finnmark Platform, the erosion decreases slightly towards the east (Fig. 4d, e). This indicates a regional trend of less erosion towards the Russian sector. In the centre of Profile A-A', the transition from the Hammerfest Basin onto the Loppa High shows no significant change in the net apparent erosion (Fig. 4g, h). This observation implies that the Loppa High was not an active structural element during the late Cenozoic erosion episodes.

From the western edge of the Loppa High (Fig. 4i, j) there is a gradual westwards decrease in the estimated net apparent erosion, best seen in the Neogene (Layers 03-07) and Paleogene (Layers 08 and 09) using the CretShale baseline. The Harstad, Tromsø, Sørvestsnaget and Bjørnøya basins are deep Cretaceous basins (Fig. 1) with massive shales. The deep Cretaceous (and parts of the deeper Paleogene) has anomalously low velocity throughout the whole area and does not conform to the CretShale baseline. The low velocity in these areas has been quality controlled and is not an artefact. One possible explanation for this is high overpressure prior to uplift and erosion, some of which may remain today. There may also be a lithology change in the Paleogene in places from shale to biogenic ooze (silica), which has lower velocity than shale and would give a significant mismatch with the CretShale baseline. Presence of ooze has been reported in well 7216/11-1S (Ryseth et al. 2003) and further north, closer to Profile A-A', in well 7316/5-1 within the Paleogene wedges (Eidvin et al. 1998). Due to these strong geological velocity variations the net apparent erosion estimates in this area are uncertain.

Profile B-B'

The layout of Profile B-B' in Figure 5a–c is similar to that for profile A-A'. This profile has a different set of interpreted horizons, and runs from north to south. The best layers for net apparent erosion are Cretaceous (Layer 06) and Triassic (Layer 10) (Fig. 5a). The velocities above the Permian are stable and there are no problems using these layers for velocity inversion analysis (Fig. 5b). On the net apparent erosion profile in Figure 5c (upper panel), well 7125/4-2 is superimposed, with estimated erosion from the sonic log method (enlarged in Figure 5d, e (Ktenas et al. 2017)). The graph in the lower panel of the figure shows stable erosion estimates from the two layers in the south, as compared to the northern and central parts of the profile, where estimates from the two layers differ significantly. The corrected map follows estimates from the Triassic (Layer 10). Apart from the mismatch between the layers, the profile shows a stable and almost linear increase in net apparent erosion towards the north.

Enlarged displays of the southern and northern parts of Profile B-B' are shown in Figure 5d–h. Figure 5d, e shows the southern section, the Nysleppen Fault Complex area, where the erosion estimates from Layers 06-Cretaceous and 10-Triassic are in good agreement. Figure 5f, g shows the northern part, the Bjarmeland Platform, where the erosion estimates from Layers 06-Cretaceous and 10-Triassic disagree. Closer inspection of the velocity inversion results indicates that the Cretaceous layer appears to have changed lithofacies such that the CretShale

‘shale’ baseline is no longer appropriate. A facies change towards a mixed sand-shale lithology is seen on Svalbard and in the Russian Barents Sea (Stoupakova et al. 2011) and is indicated by seismic observations of clinoforms farther east in the Norwegian sector (Marin et al. 2017). No wells have been drilled through the Cretaceous in this area. In the absence of a well-tie, we tested the hypothesis that the Cretaceous might consist of a mixed-sand shale lithology on the Bjarmeland Platform by plotting Layer 06-Cretaceous against the ‘mixed sand-shale’ LJurTrias baseline, as used for layer 10-Triassic. The result is shown in Figure 5h and gives a good match between the two layers. This indicates that there is a good chance of finding reservoir sands in the Cretaceous in this area.

Profile C-C’

The layout of Profile C-C’ in Figure 6a–c is similar to that for Profile A-A’. This profile has a different set of interpreted horizons and also runs from north to south. The best layers for net apparent erosion are 03-Paleogene, 04-Cretaceous and 07-Triassic (Fig. 6a). The velocities are stable above the Permian (Fig. 6b). In the deep Bjørnøya Basin, velocities are anomalously low. Figure 6c (upper panel) shows net apparent erosion along the profile, with a sonic log based erosion estimate from well 7120/2-1 superimposed (enlarged in Figure 6d, e (Ktenas et al. 2017)). The graph in the lower panel of Figure 6c shows significant disagreement between erosion estimates from the different layers of the profile. A possible reason for the uncertainty is that Profile C-C’ runs north-south close to the edge of the deep Cretaceous basins of the western Barents Sea (Fig. 1).

The quality of the net apparent erosion estimates along this profile is lower than those in the other profiles. With support from other data it is possible to make a valid interpretation of net apparent erosion along the whole length of profile C-C’ (Fig. 6c), but the same layers cannot be used everywhere. The best layer is 03-Paleogene, which matches 04-Cretaceous in the Hammerfest Basin (and therefore gives a valid estimate there with the CretShale baseline), and is stable until it pinches-out in the middle of the Bjørnøya Basin. Layer 04-Cretaceous is reliable in the Hammerfest Basin, partly over the Bjørnøya Fault Complex (the down-stepping fault blocks north of the Loppa High), and at the northern pinch-out in the Bjørnøya Basin. Layer 07-Triassic is more noisy. It is reliable over most of the Hammerfest Basin, on the Loppa High, and at the northern pinch-out edge in the Bjørnøya Basin. At the base of the Bjørnøya Basin, the layer has anomalously low velocity which gives a zero erosion estimate. This is most likely an artefact for the same reasons as discussed under Profile A-A', in the deep Cretaceous in Sørvestsnaget Basin. A possible geological mechanism is that of high overpressure prior to uplift and erosion, which some of it may remain until today. The Triassic is affected by high 'velocity leakage' from the basement (blue-green colour) in the hanging wall of the southern Loppa High boundary fault, and by low velocity leakage from the Bjørnøya Basin Cretaceous sequence in the Bjørnøya Fault Complex (red colour).

When anomalies and inaccurate erosion estimates are not taken into account, Profile C-C' shows a smooth regional trend with little variation in net apparent erosion from the Hammerfest Basin in the south and across the Loppa High. As the layers incline towards the north and start to sub-crop, from the middle of the Bjørnøya Basin and northwards, there is a marked northwards increase in erosion towards the Stappen High. The net apparent erosion values estimated at the northern edge of the profile are ~2500 m, and assuming further northwards increase, are comparable with the estimate of circa 3 km of erosion reported by Vågnes & Amundsen (1993), from analysis of samples from Bjørnøya.

Net apparent erosion map estimates in the southwestern Barents Sea

Gridded time structure maps were available for Top Paleogene, Base Tertiary, Base Cretaceous, Intra Lower Jurassic and Base Upper Triassic. These were used to perform velocity inversion for the Paleogene (with the CretShale baseline, Fig. 7), Cretaceous (with the CretShale baseline, Fig. 8), and Lower Jurassic–Upper Triassic layers (with the LJurTrias baseline, Fig. 9). The zero erosion lines drawn in Figures 7 and 8 follow the present day continental shelf break. Overall, the best net apparent erosion estimates are associated with the Cretaceous map, but there are areas where this map is invalid. In the western Barents Sea, as discussed under Profile A-A' and C-C', the Paleogene map was used in preference. On the Bjarmeland Platform, as discussed under Profile B-B, the Lower Jurassic–Upper Triassic map was used. There is also a limitation in the extent of the Cretaceous map (Fig. 8), especially towards the east, but also to the north, south and on the Loppa High. In these areas values from the Lower Jurassic–Upper Triassic map (Fig. 9) were merged in. The merged map was then calibrated to wells (Ktenas et al. 2017), as previously recommended. The calibration was performed by linear regression of erosion estimated from the sonic log method for wells (Ktenas et al. 2017, shown in Fig.10) against map erosion estimates. The correction was carried out by applying the cross-plot regression to the map. The corrected map was not tied to wells, instead the estimated differences at the well locations were measured and tabulated. The crossplot and data values are shown in Figure 11 and Table 1. The corrected map is shown in Figure 12. Some changes were made to the Intra Lower Jurassic and Base Upper Triassic map during this merging process; including clipping areas where the corrected map estimates were considered unreliable. As it is based on mid-point data, the corrected map will include some variations which are due to lithology changes rather than indications of erosion; thus the corrected map will not be reliable in detail, but large scale trends should be reliable.

An interesting observation was made at the map merge step around the Nordkapp Basin, where the Lower Jurassic–Upper Triassic map (Fig. 9) has a zone of increased velocity which gives an impression of increased net apparent erosion. However, this is not seen for the Cretaceous (Fig. 8). We believe that this might be related to a diagenetic effect caused by enhanced vertical fluid flow through the more sandy Triassic and Jurassic section in the vicinity of the salt diapirs.

Comparison of map based inversion with well log methods

Velocity inversion of time structure maps using a high quality regional velocity model gives an areally continuous estimate of net apparent erosion (Fig. 12). The well log based method is more accurate, but produces a sparse data set from which it can be difficult to make a reliable map (Fig. 10). Comparison of the maps from the two different methods shows great similarities. The trends of decreasing net apparent erosion towards the west in the western Barents Sea, and of increasing erosion towards the north in the central study area, are similar. These appear to be fairly smooth regional trends which the sparse well data set has enough resolution to capture.

Closer comparison of the two maps reveals trends which the well log study fails to reflect. There is a clear relationship between the density of well data and the ability of the well study to capture trends. At the eastern edge of the study area, the map based inversion picks up decreasing net apparent erosion towards the Olga Basin in the Russian Barents Sea (east of our study area, NPD 2017), and the erosion isocontours swing around to a northerly direction. West of this, in the central-northern area, the isocontours have a NE-SW direction. The overall trend in Figure 12 shows a subtle axis of higher erosion trending towards the NW (towards Svalbard). This trend is also visible in the estimated tectonic uplift map of Vågnes & Amundsen (1993), which includes Svalbard. Their map overlaps the northern section of our study area. This indicates that there is a major change in the crustal uplift pattern at the transition from the Norwegian mainland to the Barents Sea. The up-to-the-west tilt of the Norwegian mainland does not seem to continue into the Barents Sea. In particular, there are no traces of an up-to-the-west tilt connecting the mainland with Bjørnøya and Svalbard. While there is an obvious similarity between these areas, both the southwestern Barents Sea and the adjacent Norwegian mainland have been significantly uplifted and eroded during the late Cenozoic. The axis of the uplift, and perhaps also the timing and magnitude, appears to differ.

Investigation of details in the corrected net apparent erosion map shows features like the small apparent 'high erosion ridge' (green in Fig. 12) running NE-SW through well 7122/2-1. The corrected map based net apparent erosion estimate in this well (Table 1) is 2072 m, 472 m higher than the well estimate of 1600 m. The apparent 'ridge' is most likely a geological feature where the assumptions in the mid-point inversion methods are invalid. It seems that this feature also crosses another well, 7224/7-1 where the erosion estimate is 269 m too high. This feature is very local, and the broader area of the map around well 7122/2-1 shows lower erosion values (yellow) which appear to be regionally consistent and better aligned with the wells estimates. In well 7222/11-1 T2, the nearest well to 7122/2-1 on the map, the corrected map estimate is 1629 m, only 29 m different from the well study estimate of 1600 m.

There are three areas with a generally poor match between the well and map predictions. The first is the western Barents Sea, around wells 7019/1-1, 7117/9-1, 7119-7-1, 7216/11-1 S and 7316/5-1. These are in the area where the map erosion estimates are taken from the Paleogene. The first three wells have Paleogene and Cretaceous present, and the Cretaceous shales have been aligned with the CretShale baseline. The last two wells are far to the west, have no Cretaceous section present, and were aligned with the Paleogene (Ktenas et al. 2017). The poor match may be related to variations in lithology and/or pore pressure within the Paleogene. The second area is in the Fingerdjupet Sub-basin, around wells 7321/7-1 and 7321/8-1. The well estimates here are determined from alignment of both the Cretaceous and Triassic against their respective baselines (Ktenas et al. 2017) and appear to be of good quality.

The third area is in the Nysleppen Fault Complex area, around wells 7124/3-1 and 7125/4-2. Both well estimates come from alignment of both the Cretaceous and Triassic and appear to be good quality (Ktenas et al. 2017). The map (and profile B-B') inversion appears reasonable, but there is a difference in the detail of the results. The wells are located at the south-eastern edge of the Hammerfest Basin, near the Finnmark coast where the sedimentary section is thin. There may be some velocity leakage into the Cretaceous which affects the map inversion, especially if the time maps were not accurately interpreted.

Discussion

The corrected map of net apparent erosion in the southwestern Barents Sea (Fig.12) has many similarities with those of others (e.g. Vågnes & Amundsen 1993; Henriksen et al. 2011a; Baig et al. 2016; Johansen 2016), both in terms of regional variation (shape) and magnitude. There is a general consensus around the large scale trends: the declining erosion towards the west in the Western Barents Sea, the northwards increase in erosion, and for those with a large enough study area, the decrease towards the Olga Basin in the Russian Barents Sea with a change to approximately north-south directed erosion isocontours in the proximity of the Norway-Russia maritime border. Some studies have mapped this out over larger areas, up to and including Svalbard (Vågnes & Amundsen 1993; Henriksen et al. 2011a). Data commonly used are seismic (interpretation), compaction (velocity from seismic and wells), vitrinite reflectance and apatite fission track analysis. Important contributions have also been made using other input data such as gravity (Cochran & Talwany 1978) and apatite U-Th/He thermochronology (Zattin et al.

2016). Each data type sheds light on a different aspect of the uplift and erosion history of the area (Anell et al. 2009).

The difference in this study is not in the fundamental method, but in how it has been applied. Multi-parameter velocity inversion with a two lithology NCT model is a better approach than single lithology compaction methods. To the best of our knowledge, this is the first documented work applying this method in the Barents Sea, and the corrected net apparent erosion map is more detailed and perhaps more precise in comparison to other published maps.

Compaction based erosion estimation using velocity data is the only available method away from wells. At the wells, there is a choice to establish the baseline to which the map based erosion estimates were calibrated. We considered two methods, vitrinite reflectance and compaction (Ktenas et al. 2017). Darkening of organic particles, measured as vitrinite reflectance, happens as a consequence of time and temperature, and the influence of time is significant. The advantage of the method is that older tectonic episodes (when associated with high heat flow) can be detected. The disadvantage, in terms of net apparent erosion estimates, is that vitrinite reflectance depends on the heat flow history, the thermal conductivity of the layers (i.e. the modelled rock types), as well as the timing and magnitude of erosion, all of which have to be estimated from the calibration of observed and modelled vitrinite reflectance. The relationship between compaction, velocity and net apparent erosion relies on fewer assumptions, and the relevant parameters are easier to determine (i.e. zero erosion reference wells in similar lithology). Compaction based estimates of net apparent erosion are therefore normally more reliable (Japsen 2000; Anell et al. 2009), and hence this compaction method was adopted for our study.

A key element in this study was the use of a high quality regional velocity model for the profile and map based erosion estimates. These estimates are critically dependent on the velocity data used. Another key element was to choose layers which were unaffected by high velocity contrast boundaries such as salt domes or the top of Permian carbonates. Regional time maps and velocity models are never precise, and high (or low) velocities have a tendency to 'leak', vertically or horizontally, some distance away from such boundaries (such as at faults).

The net apparent erosion observed in the southwestern Barents Sea is a consequence of tectonic uplift. The shape of the erosion map gives some insight into the possible mechanisms and timing of this process. Taking into account previous studies, we consider regional, isostatic uplift related either to a temperature increase in the mantle and/or chemical alteration of the base of the lithosphere to be likely. For basin modelling, we propose to describe the late Cenozoic uplift and erosion history as two phases of erosion, one prior to and one after the deposition of the Pleistocene deposits in the study area. There are prominent seismic unconformities to which these phases can be correlated (e.g. Profile A-A', Fig. 4a).

Conclusions

This study shows that a rigorous application of compaction based erosion estimates, such as in multi-parameter velocity inversion with baselines for two lithologies, together with a high quality regional velocity model and time structure maps, can be used to produce net apparent erosion maps of high quality. The use of two baselines also allowed a larger geographical area to be studied, such as the northern and northeastern part of the study area where the estimates are mainly based on the Triassic. The use of several layers together in the same location also allows, in some cases, other geological parameters to be interpreted: such as the likely lithofacies change to a mixed sand and shale in the Cretaceous in the Bjarmeland Platform, and the possible diagenetic effects in the Lower Jurassic to Upper Triassic around the Nordkapp Basin. Both areas may be important for oil and gas exploration.

The regional map of net apparent erosion (Fig. 12) which has been produced for the southwestern Barents Sea is primarily consistent with similar published maps with an overprint of detail. The shape (regional variation) of the map will be an important input for petroleum migration studies as it indicates the area tilted during tectonic uplift, showing the direction of migration prior to uplift. Uncertainty is related to lithological variation, compaction disequilibrium in shales and fluid/gas fill in the sediment pore spaces.

Acknowledgements and Funding

The research leading to these results has received funding from the People Programme (Marie Curie Actions) of the European Union’s Seventh Framework Programme FP7/2007-2013/ under REA grant agreement No 317217. The research forms part of the GLANAM (GLAciated North Atlantic Margins), www.glanam.org Initial Training Network. This also corresponds to a contribution to the RCN funded project "Research Centre for Arctic Petroleum Exploration" (ARCEx) (Grant 228107). We are thankful to First Geo AS and Olav Egeland for allowing us to use the Geocap and AKGT data, software and methods. We sincerely thank the Co-Editor Jo Prigmore, Alan Roberts, Roman Spitzer and one anonymous reviewer for thorough and constructive feedback during the review process. We are grateful to Alexandros Tasianas and Ben Manton for comments, which helped to improve the English of the manuscript. Thanks to NPD, Spectrum, TGS NOPEC ASA and Searcher Seismic, for permission to publish the seismic data. Furthermore, we would like to thank North E&P (North Energy Norge AS) for permission to use their internal time interpretation from the southwestern Barents Sea.

References

Andreassen, K. & Winsborrow, M. 2009. Signature of ice streaming in Bjørnøyrenna, Polar North Atlantic, through the Pleistocene and implications for ice-stream dynamics. *Annals of Glaciology*, **50**(52), 17–26.

Anell, I.A.M., Thybo, H. & Artemieva, I. 2009. Cenozoic uplift and subsidence in the North Atlantic region: geological evidence revisited. *Tectonophysics*, **474**(1–2), 78–105. doi: 10.1016/j.tecto.2009.04.006.

Baig, I., Faleide, J.I., Jahren, J. & Mondol, N.H. 2016. Cenozoic exhumation on the southwestern Barents Shelf: estimates and uncertainties constrained from compaction and thermal maturity analyses. *Marine and Petroleum Geology*, **73**, 105–130.

Bellwald, B., Planke, S., Piasecka, E.D., Matar, M.A. & Andreassen, K. 2018. Ice-stream dynamics of the SW Barents Sea revealed by high-resolution 3D seismic imaging of glacial deposits in the Hoop area. *Marine Geology*, **402,** 165–183. doi: 10.1016/j.margeo.2018.03.002.

Cavanagh, A.J., di Primio, R., Scheck-Wenderoth, M. & Horsfield, B. 2006. Severity and timing of Cenozoic exhumation in the southwestern Barents Sea. *J. Geol. Soc.,* **163**, 761–774.

Cochran, J.R. & Talwani, M. 1978. Gravity anomalies, regional elevation, and the deep structure of the North Atlantic. *Journal of Geophysical Research: Solid Earth*, **83**(B10), 4907-4924.

Dimakis, P., Braathen, B.I., Faleide, J.I., Elverhoi, A. & Gudlaugsson, S.T. 1998. Cenozoic erosion and the preglacial uplift of the Svalbard–Barents Sea region. *Tectonophysics,* **300**, 311–327.

Doré, A.G. & Jensen, L.N. 1996. The impact of late Cenozoic uplift and erosion on hydrocarbon exploration: offshore Norway and some other uplifted basins. *Global and Planetary Change*, **12**(1–4), 415–436.

Dræge, A., Duffaut, K., Wiik T. & Hokstad, K. 2014. Linking rock physics and basin history—Filling gaps between wells in frontier basins. *The Leading Edge*, **33**(3), 240–246.

Duran, E.R., di Primio, R., Anka, Z., Stoddart, D. & Horsfield, B. 2013. 3D-basin modelling of the Hammerfest Basin (southwestern Barents Sea): A quantitative assessment of petroleum generation, migration and leakage. *Marine and Petroleum Geology*, **45**, 281–303.

Eidvin, T., Goll, R.M., Grogan, P., Smelror, M. & Ulleberg, K. 1998. The Pleistocene to Middle Eocene stratigraphy and geological evolution of the western Barents Sea continental margin at well site 7316/5-1 (Bjørnøya West area). *Norsk Geologisk Tidsskrift*, **78**, 99–124.

Eidvin, T., Jansen, E., Riis, F. 1993. Chronology of Tertiary fan deposits off the western Barents Sea: implications for the uplift and erosion history of the Barents Shelf. *Marine Geology*, **112**, 109–131.

Faleide, J.I., Tsikalas, F., Breivik, A.J., Mjelde, R., Ritzmann, O., Engen, O., Wilson, J., Eldholm, O. 2008. Structure and evolution of the continental margin off Norway and the Barents Sea. *Episodes*, **31**, 82–91.

Faleide, J.I., Solheim, A., Fiedler, A., Hjelstuen, B.O., Andersen, E.S. & Vanneste, K. 1996. Late Cenozoic evolution of the western Barents Sea-Svalbard continental margin. *Global Planetary Change*, **12**, 53–74.

Faleide, J.I., Vagnes, E. & Gudlaugsson, S.T. 1993. Late Mesozoic-Cenozoic evolution of the southwestern Barents Sea in a regional rift-shear tectonic setting. *Marine and Petroleum Geology*, **10**, 186–214.

First Geo 2017. Regional High Quality Velocity cube for the Barents Sea, Norwegian Sector. (Commercially confidential database, unpublished).

Gabrielsen, R.H., Faerseth, R.B. & Jensen, L.N. 1990. Structural Elements of the Norwegian Continental Shelf. Pt. 1. The Barents Sea Region. Norwegian Petroleum Directorate.

Gardner, G.H.F., Gardner, L.W. & Gregory, A.R. 1974. Formation velocity and density - diagnostic basics for stratigraphic traps. *Geophysics*, **39**, 770–780.

Gateman, H. & Avseth, P. 2016. Net uplift estimation using both sandstone modeling and shale trends, on the Horda Platform area in the Norwegian North Sea. In: SEG Technical Program Expanded Abstracts 2016 (pp. 3288–3292). Society of Exploration Geophysicists.

Gradstein, F.M., Anthonissen, E., Brunstad, H., Charnok, M., Hammer, O. Hellem, T. & Lervik, K.S. 2010. Norwegian offshore stratigraphic lexicon (NORLEX). *Newsletter on Stratigraphy*, **44**(1), 73–86.

Green, P.F., Duddy, I.R., 2010. Synchronous exhumation events around the Arctic including examples from Barents Sea and Alaska North Slope. In: Vining, B.A., Pickering, S.C. (eds) Petroleum Geology: from Mature Basins to New Frontiers – Proceedings of the 7th Petroleum Geology Conference, London. Geological Society, London, pp. 633–644.

Henriksen, E., Bjørnseth, H.M., Hals, T.K., Heide, T., Kiryukhina, T., Klovjan, O.S., Larssen, G.B., Ryseth, A.E., Rønning, K., Sollid, K. & Stoupakova, A. 2011a. Uplift and erosion of the greater Barents Sea: impact on prospectivity and petroleum systems. In: Spencer, A.M., Embry, A.F., Gautier, D.L., Stoupakova, A.V. & Sorensen, K. (eds) Arctic Petroleum Geology. *Geological Society of London Memoir* **35**, London, pp. 271–281.

Henriksen, E., Ryseth, A.E., Larssen, G.B., Heide, T., Rønning, K., Sollid, K. & Stoupakova, A.V. 2011b. Tectonostratigraphy of the greater Barents Sea: implications for petroleum systems. In: Spencer, A.M., Embry, A.F., Gautier, D.L., Stoupakova, A.V. & Sørensen, K. (eds) Arctic Petroleum Geology. *Geological Society of London Memoir* **35**, London, pp. 163–195.

Hubred, J.H. & Meisingset, I. 2013. Passive margin play and prospect evaluation using regional depth seismic and inversion of seismic processing velocities. In: EAGE/AAPG Workshop on Basin-Margin Wedge Exploration Plays. Lisbon, Portugal.

Japsen, P. 2000. Investigation of multi-phase erosion using reconstructed shale trends based on sonic data. Sole Pit axis, North Sea. *Global Planetary Change*, **24**, 189–210.

Japsen, P., Mukerji, T. & Mavko, G. 2007. Constraints on velocity-depth trends from rock physics models. *Geophysical Prospecting*, **55**, 135–154.

Japsen, P. 2018. Sonic velocity of chalk, sandstone and marine shale controlled by effective stress: Velocity-depth anomalies as a proxy for vertical movements. *Gondwana Research,* **53**, 145–158.

Johansen, F., Meisingset, I., Leven, J. & Coker, J. 2015. Geopressure variations within the North West Shelf from well analysis and the regional hiQbe™ velocity model. ASEG Extended Abstracts 2015: 24th International Geophysical Conference and Exhibition: pp. 1–2.

Johansen, N.S. 2016. Regional net erosion estimations and implications for seismic AVO signatures in the western Barents Sea. M.Sc. thesis, Norwegian University of Science and Technology (NTNU), Trondheim, pp. 1–178.

Knies, J., Matthiessen, J., Vogt, C., Laberg, J.S., Hjelstuen, B.O., Smelror, M., Larsen, E., Andreassen, K., Eidvin, T. & Vorren, T.O. 2009. The Plio-Pleistocene glaciation of the Barents Sea–Svalbard region: a new model based on revised chronostratigraphy. *Quaternary Science Reviews,* **28**, 812–829.

Ktenas, D., Henriksen, E., Meisingset, I., Nielsen, J.K. & Andreassen, K. 2017. Quantification of the magnitude of net erosion in the southwest Barents Sea using sonic logs and compaction trends in shales and sandstones. *Marine and Petroleum Geology*, **88**, 826–844.

Laberg, J.S., Andreassen, K. & Vorren, T.O. 2012. Late Cenozoic erosion of the high latitude southwestern Barents Sea Shelf revisited. The Geological Society of America Bulletin, **124**, 77–88.

Lasabuda, A., Laberg, J.S., Knutsen, S.M. & Safronova, P. 2018. Cenozoic tectonostratigraphy and pre-glacial erosion: A mass-balance study of the northwestern Barents Sea margin, Norwegian Arctic. *Journal of Geodynamics*, Special Arctic Issue. doi: 10.1016/j.jog.2018.03.004

Marin, D., Escalona, A., Śliwińska, K.K., Nøhr-Hansen, H. & Mordasova, A. 2017. Sequence stratigraphy and lateral variability of Lower Cretaceous clinoforms in the southwestern Barents Sea. *AAPG Bulletin*, **101**(9), 1487–1517.

Meisingset, I., Coker, J. & Leven, J. 2017. Geo-pressure on the Australian North West Shelf. In First EAGE Workshop on Pore Pressure Prediction, Pau, France.

Meisingset, I., Hubred, J. & Krasova, D. 2018. High quality regional velocity modelling for depth conversion. In: First EAGE/PESGB Workshop on Velocities, London.

Mukerji, T., Dutta, N., Prasad M. & Dvorkin, J. 2002. Seismic detection and estimation of overpressures, Part I: The rock physics basis: CSEG Recorder, **27**, no. 7, 34–57.

Nielsen, J.K., Ktenas, D., Henriksen, E., Holm, D.H., Kaikas, E., Samu, L. & Samuelsberg, T. 2015. Impact of ice ages and tectonic activity on the petroleum systems of the western Barents Sea. In: 3P Arctic: The Polar Petroleum Potential Conference and Exhibition. American Association of Petroleum Geologists (AAPG), Stavanger, Norway.

NPD 2016. Barents Sea Structural Elements Map. Norwegian Petroleum Directorate (NPD), Stavanger, Norway, http://gis.npd.no/factmaps/html_20/ [last accessed January 2018].

NPD 2017. Structural and stratigraphic overview of Barents Sea North. Norwegian Petroleum Directorate (NPD), Stavanger, Norway, http://www.npd.no/en/Publications [last accessed June 2018].

Peikert, E.W. 1985. Stratigraphic velocity interpretation: National Petroleum Reserve—Alaska. Seismic stratigraphy II: An integrated approach to hydrocarbon exploration: *AAPG Memoir*, **39**, 7–36.

Richardsen, G., Vorren, T. & Tørrudbaken, B.O. 1993. Post-Early Cretaceous uplift and erosion in the southern Barents Sea: a discussion based on analysis of seismic interval velocities. *Norsk Geologisk Tidsskrift*, **73**, 3–20.

Riis, F. & Fjeldskaar, W. 1992. On the magnitude of the late Tertiary and Quaternary erosion and its significance for the uplift of Scandinavia and the Barents Sea. In: Larsen, R.M., Brekke, Ritzmann, O. & Faleide, J.I. (eds) 2009. The crust and mantle lithosphere in the Barents Sea-Kara Sea region. *Tectonophysics*, **470**, 89–104.

Ryseth, A., Augustson, J.H., Charnock, M., Haugerud, O., Knutsen, S.M., Midbøe, P.S., Opsal, J.G. & Sundsbø, G. 2003. Cenozoic stratigraphy and evolution of the Sørvestsnaget Basin, southwestern Barents Sea. *Norsk Geologisk Tidsskrift*, **83**, 107–130.

Rønnevik, H. & Jacobsen, H.P. 1984. Structural highs and basins in the western Barents Sea. In: Spencer, A.M. (ed.), Petroleum Geology of North European Margin. *Norwegian Petroleum Society*, pp. 98–107.

Schlumberger Limited 2009. Schlumberger Log Interpretation Charts, Por 1-2, Sonic Tool, 212–213.

Sclater, J.G. & Christie, P.A. 1980. Continental stretching: An explanation of the post Mid-Cretaceous subsidence of the central North Sea Basin. *Journal of Geophysical Research: Solid Earth*, **85**(B7), 3711–3739.

Storvoll, V., Bjørlykke, K. & Mondol, N.H. 2005. Velocity-depth trends in Mesozoic and Cenozoic sediments from the Norwegian Shelf. *AAPG Bulletin*, **89**(3), 359–381.

Stoupakova, A.V., Henriksen, E., Burlin Y.K., Larsen G.B., Milne J.K., Kiryukhina, T.A., Golynchik, P.O., Bordunov S.I, Ogarkova M.P. & Suslova, A.A. 2011. The geological evolution and hydrocarbon potential of the Barents and Kara shelves. In: Spencer, A.M., Embry, A.F., Gautier, D.L., Stoupakova, A.V. & Sørensen, K. (eds) Arctic Petroleum Geology. *Geological Society of London Memoir* **35**, London, pp. 325–344. Doi: https://doi.org/10.1144/M35.21.

Tsikalas, F., Faleide, J.I., Eldholm, O. & Blaich, O.A. 2012. The NE Atlantic conjugate margins. In: Roberts, D.G., Bally, A.W. (eds), Regional Geology and Tectonics: Phanerozoic Passive Margins, Cratonic Basins and Global Tectonic Maps. Elsevier, pp. 140–201.

Vorren, T.O., Richardsen, G., Knutsen, S.-M. & Henriksen, E. 1991. Cenozoic erosion and sedimentation in the western Barents Sea. Marine and Petroleum Geology, 8, 317–340.

Vågnes, E. & Amundsen, H.E.F. 1993. Late Cenozoic uplift and volcanism on Spitsbergen: Caused by mantle convection? *Geology*, **21**(3), 251–254.

Zattin, M., Andreucci, B., de Toffoli, B., Grigo, D. & Tsikalas, F. 2016. Thermochronological constraints to late Cenozoic exhumation of the Barents Sea Shelf. *Marine Petroleum Geology* **73**, 97–104.

Zieba, K.J., Daszinnies, M., Emmel, B., Lothe, A., Grøver, A. & Lippard, S. 2014. Assessment of the Cenozoic erosion amount using Monte Carlo type-petroleum systems modeling of the Hammerfest Basin, western Barents Sea. *American Journal of Geoscience*, **4**, 40–53.

Figure Captions

Fig. 1. Map of the Norwegian Barents Sea showing the different structural elements and oil-

gas discoveries. The regional seismic Profiles A-A', B-B' and C-C' and the wells studied along the lines are indicated with red lines and red dots, respectively. The location of the study area is indicated in the inserted figure. Modified after Norwegian Petroleum Directorate (NPD 2016).

Fig. 2. Generalized lithostratigraphic chart illustrating the approximate age, lithologies and major geodynamic events. Modified after Norwegian Interactive Offshore Stratigraphic Lexicon (NORLEX) (Gradstein et al. 2010).

Fig. 3. Conceptual model for the estimation of net apparent erosion (**a**) two layers of Cretaceous (green) and Lower Jurassic–Upper Triassic age (yellow) with their layer mid-points superimposed (**b**) the Dikte NCT model of Ktenas et al. (2017) applied in this study, where the CretShale baseline is representative for Cretaceous shales and the LJurTrias baseline is representative for Lower Jurassic–Triassic rocks with mixed sand-shale lithologies deposited in a coastal plain to shallow marine environment. Net apparent erosion is calculated as the vertical depth difference between the layer's baseline, where the layer would have been at maximum depth of burial, and the present depth of burial.

Fig. 4. Profile A-A'. (**a**) Regional depth converted geoseismic Profile A-A' running from the northwest to the southeast illustrating areas with missing section and major erosion. (**b**) Interval velocity profile from the regional Barents Sea velocity cube along the plane of the profile. (**c**) Net apparent erosion for the Neogene, Paleogene, Cretaceous and Lower Jurassic–Upper Triassic stratigraphic intervals in two panels, a seismic section with colour overlay and a graph. Erosion estimates from wells 7124/3-1, 7222/11-1 and 7220/8-1 are superimposed. The graph shows estimated erosion from each of the inverted layers. Net apparent erosion from the

corrected map (shown in Figure 12) is included for comparison. (**d & e**) Enlarged southeastern part of the profile over the Finnmark Platform. (**f**) Enlarged inverted layers in the southeastern part of the profile illustrating the sensitivity of the velocity analysis. (**g & h**) Enlarged central part of the profile over the Loppa High and Hammerfest Basin. (**j & i**) Enlarged westernmost part of the profile over the Sørvestsnaget Basin.

Fig. 5. Profile B-B'. (**a**) North-south regional depth converted geoseismic Profile B-B' across the Finnmark Platform and Bjarmeland Platform. (**b**) Interval velocity profile from the regional Barents Sea velocity cube along the plane of the profile. (**c**) Net apparent erosion for the Cretaceous and Lower Jurassic–Upper Triassic stratigraphic intervals in two panels, a seismic section with colour overlay and a graph. On the Finnmark Platform, erosion estimates from well 7125/4-2 is superimposed. The graph shows estimated erosion from each of the inverted layers. Net apparent erosion from the corrected map (shown in Figure 12) is included for comparison. (**d & e**) Enlarged southern part of the profile, over the Finnmark Platform and Nysleppen Fault Complex. (**f & g**) Enlarged northern part of the profile, over the Bjarmeland Platform. (**h**) As above, with Cretaceous on Triassic baseline.

Fig. 6. Profile C-C'. (**a**) North-south regional depth converted geoseismic Profile C-C' across the Finnmark Platform and Bjarmeland Platform. (**b**) Interval velocity profile from the regional Barents Sea velocity cube along the plane of the profile. (**c**) Net apparent erosion for the Jurassic and Lower Jurassic–Upper Triassic stratigraphic intervals in two panels, a seismic section with colour overlay and a graph. The graph shows estimated erosion from each of the inverted layers. Net apparent erosion from the corrected map (shown in Figure 12) is included for comparison. On the Loppa High, the erosion estimate of the well 7120/2-1 is superimposed on top of the profile and enlarged in (**d** & **e**). The low velocity and net

apparent erosion estimates, which are close to zero in the Bjørnøya Basin within the Cretaceous and Triassic intervals, may indicate an area of overpressure (i.e. gas movement in sandstones).

Fig. 7. Regional net apparent erosion map for the Paleogene interval in the southwestern Barents Sea. The zero erosion line was established based on the present geomorphology of the seabed.

Abbreviations of the structural elements: BB, Bjørnøya Basin; BFC, Bjørnøyrenna Fault Complex; BP, Bjarmeland Platform; FSB, Fingerdjupet Sub-basin; HB, Harstad Basin; HFB, Hammerfest Basin; HA, Hopenbanken Arch; HFC, Hoop Fault Complex; HFZ, Hornsund Fracture Zone; FP, Finnmark Platform; LH, Loppa High; MB, Maud Basin; MH, Mercurius High; NFC, Nysleppen Fault Complex; NH, Norsel High; NKB, Nordkapp Basin; PSP, Polheim Sub-platform; RLFC, Ringvassøy-Loppa Fault Complex; SD, Samson Dome; Sv.D, Svalis Dome; SFZ, Senja Fracture Zone; SG, Swaen Graben; SH, Stappen High; SNB, Sørvestsnaget Basin; SR, Senja Ridge; TB, Tromsø Basin; VH, Veslemøy High; VVP, Vestbakken Volcanic Province.

Fig. 8. Regional net apparent erosion map for the Cretaceous interval. In SNB, TB, VH, HB and southern BB, the extracted net erosion estimates (close to zero) are erroneous. On the Loppa High the net erosion is not calculated and the salt domes in NKB are indicated with a grey colour. The zero erosion line was established based on the present geomorphology of the seabed. For the abbreviations of the structural elements see the caption of Figure 7.

Fig. 9. Net apparent erosion map for the Triassic interval. The net erosion estimates from sonic logs utilising by the Dikte NCT model are superimposed for comparison. A large part of the NKB including the salt domes is not interpreted and is indicated with a grey color. For the

abbreviations of the structural elements see the caption of Figure 7. FH, Fedinsky High; PFC, Polstjerna Fault Complex; TIFC, Thor Iversen Fault Complex; VD, Veslekari Dome.

Fig. 10. Regional net apparent erosion map based on sonic velocity log data (modified after Ktenas et al. 2017). The map was gridded from the illustrated well points and clipped to the area of Figure 8. For the abbreviations of the structural elements see the caption of Figures 7 and 9.

Fig. 11. Crossplot of the net apparent erosion estimates in wells against the values from the merged map at well locations. The X-axis corresponds to map estimates and the Y-axis to the well estimates. The regression (correction) formula is $Y = 0.7975*X + 400$.

Fig. 12. Corrected net apparent erosion map derived from the inverted maps (Paleogene, Cretaceous and Triassic) and the net apparent erosion based on the well-log method. The wells 7128/4-1 and 7128/6-1 are not included in the calculation. For the abbreviations of the structural elements see the caption of Figures 7 and 9.

Table 1. Net apparent erosion estimates from two independent methods, based on the well-log study (Ktenas et al. 2017) and the map before and after the correction. The differential net erosion estimates illustrate the uncertainties. For the location of the wells see Fig. 12.

Well name	Well estimates (m) (Ktenas et al. 2017)	Map estimates from velocity inversion (m)	Corrected map estimates (m)	Map estimation error (±m); well minus corrected map
7019/1-1	1800	1381	1501	299
7117/9-1	1000	449	758	242
7119-7-1	1750	1228	1380	370
7120/1-1 R2	1750	1824	1855	-105
7120/12-1	1600	1192	1350	250
7120/12-2	1600	1355	1481	119
7120/2-1	1750	1857	1881	-131
7120/9-2	1700	1396	1513	187
7121/5-1	1650	1628	1699	-49
7121/5-2	1750	1681	1741	9

7121/5-3	1700	1534	1623	77
7121/9-1	1650	1592	1669	-19
7122/2-1	1600	2096	2072	-472
7124/3-1	1400	1722	1774	-374
7125/4-2	1400	1599	1675	-275
7128-4-1	1450	Not covered by map		
7128-6-1	1500	Not covered by map		
7216/11-1 S	361	430	743	-382
7220/8-1	1750	1644	1711	39
7222/11-1 T2	1600	1541	1629	-29
7224/7-1	1600	1842	1869	-269
7228/2-1 S	2250	2005	1999	251
7228/9-1 S	2000	1795	1831	169
7229/11-1	1700	1742	1789	-89
7316/5-1	800	1025	1218	-418
7321/7-1	2500	2225	2175	325
7321/8-1	2200	1846	1872	328
7324/10-1	2100	2212	2164	-64
			Average	0
			Standard deviation	252

Figure 1

Click here to access/download;figure;Figure 1_Study area.jpg

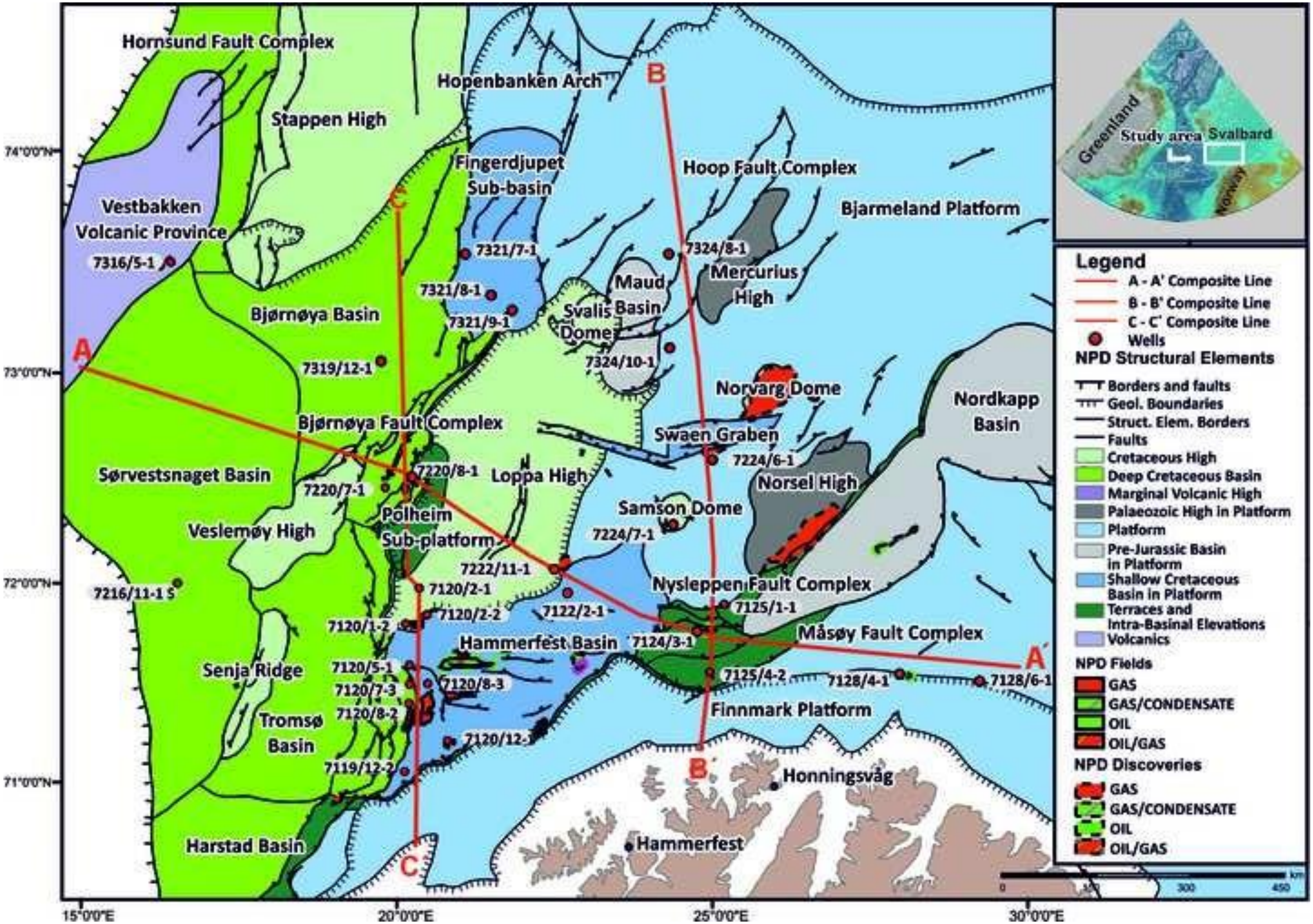

figure 2 Click here to access/download;figure;Figure_2.jpg

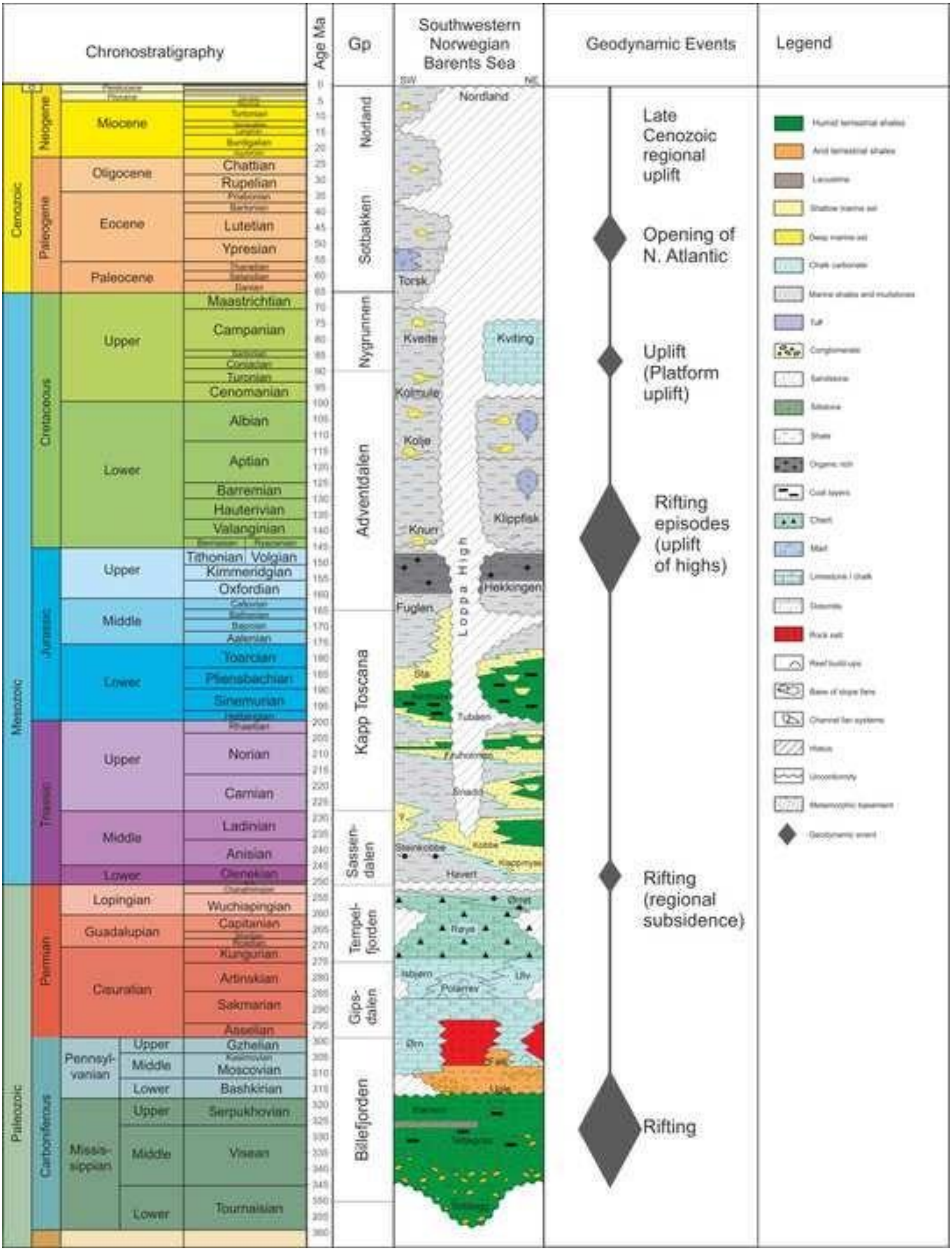

Figure 3

Click here to access/download;figure;Figure 3_Conceptual model.jpg

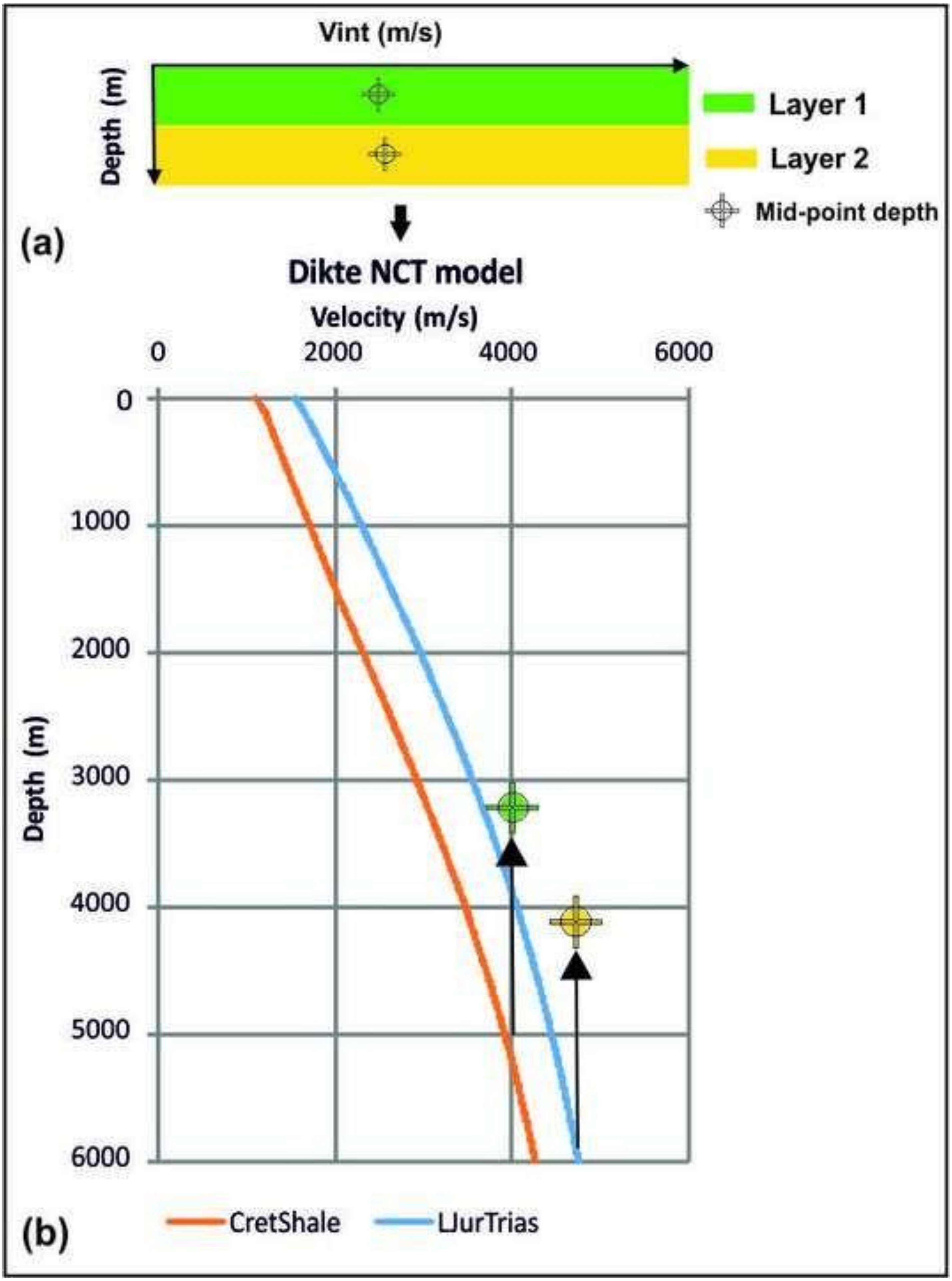

Figure 4a

Click here to access/download;figure;Figure 4a_Profile A-A_Geoseismic.jpg

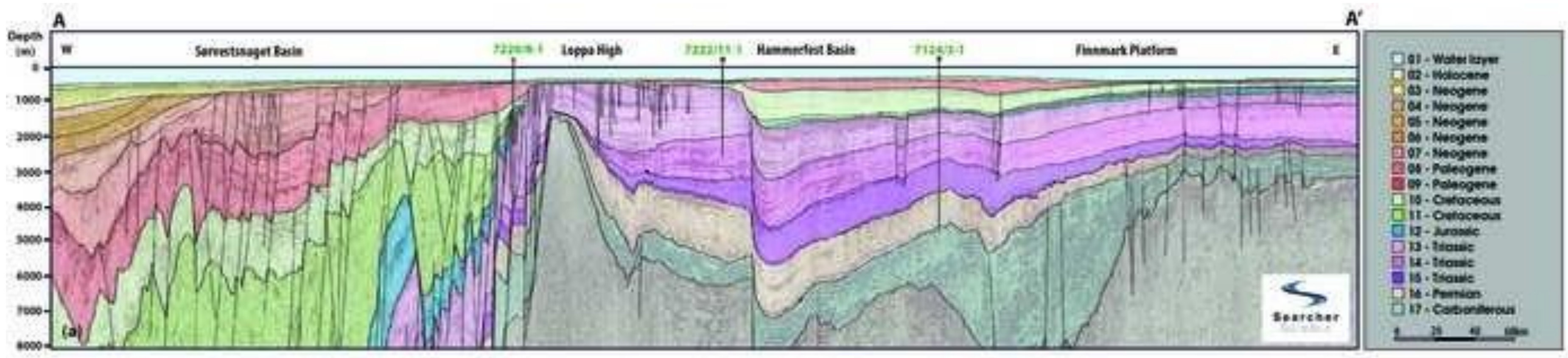

Figure 4b

Click here to access/download;figure;Figure 4b_Profile A-A_Velocity.jpg

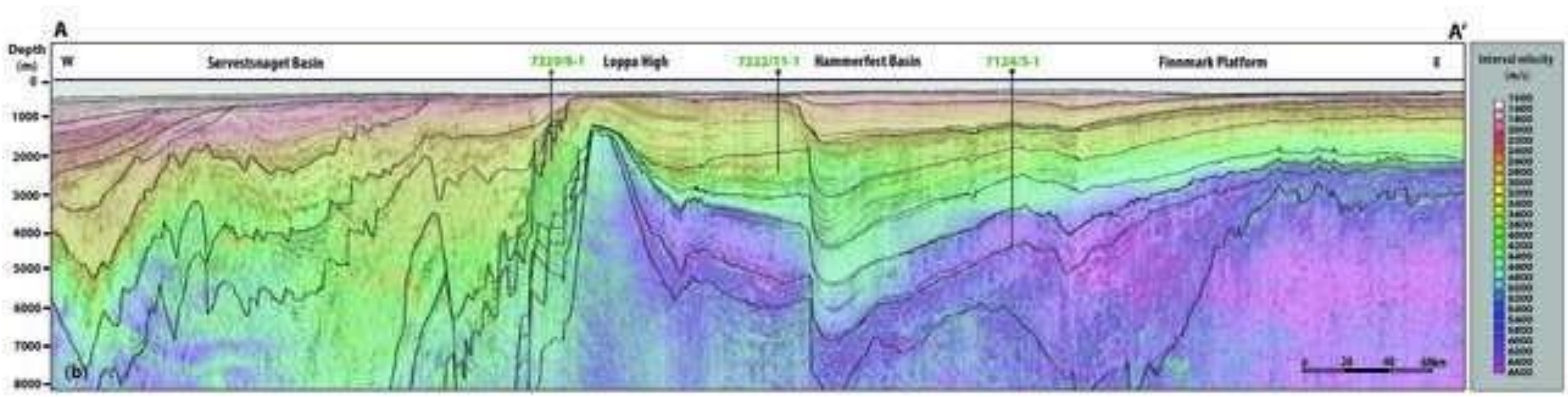

Figure 4c upper panel

Click here to access/download;figure;Figure 4c_Profile A-A_Erosion.jpg

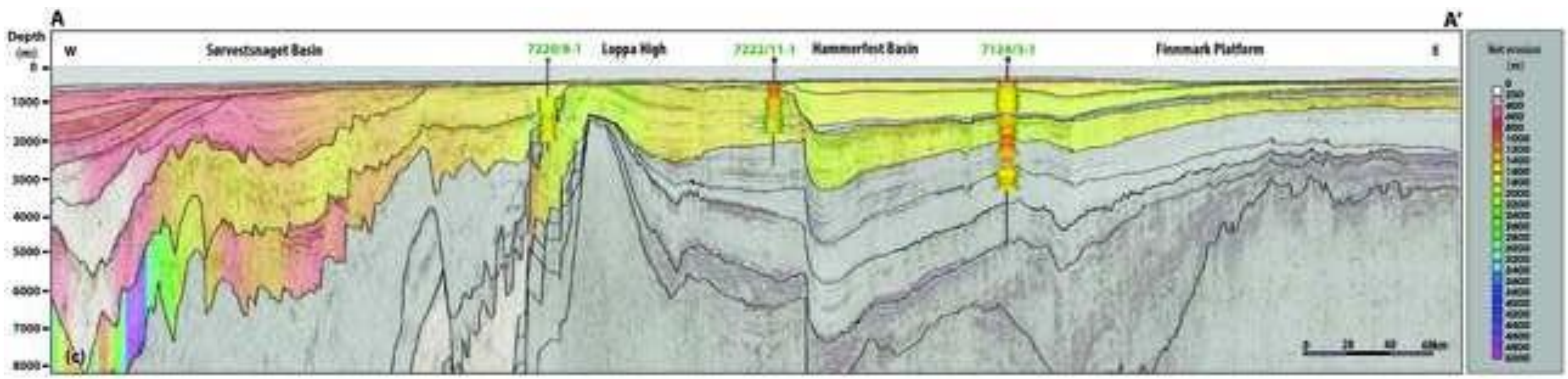

figure 4c lower panel

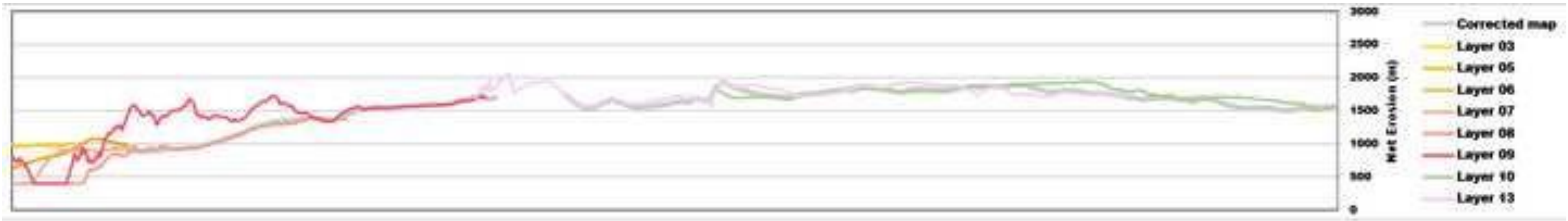

Figure 4d

Click here to access/download;figure;Figure 4d_Profile A-A_Geoseismic_Zoom_East.jpg

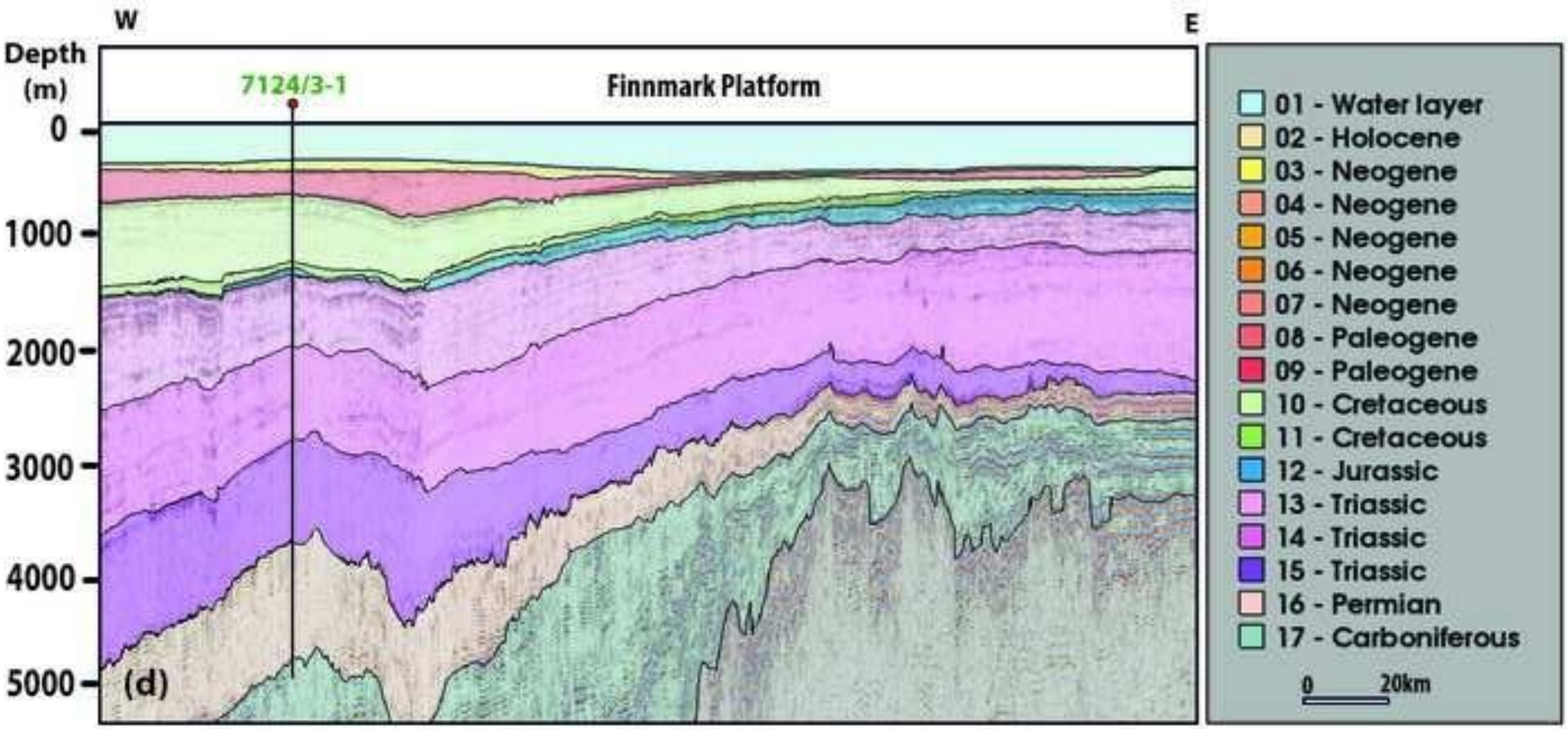

Figure 4e

Click here to access/download;figure;Figure 4e_Profile A-A_Erosion_Zoom_ East.jpg

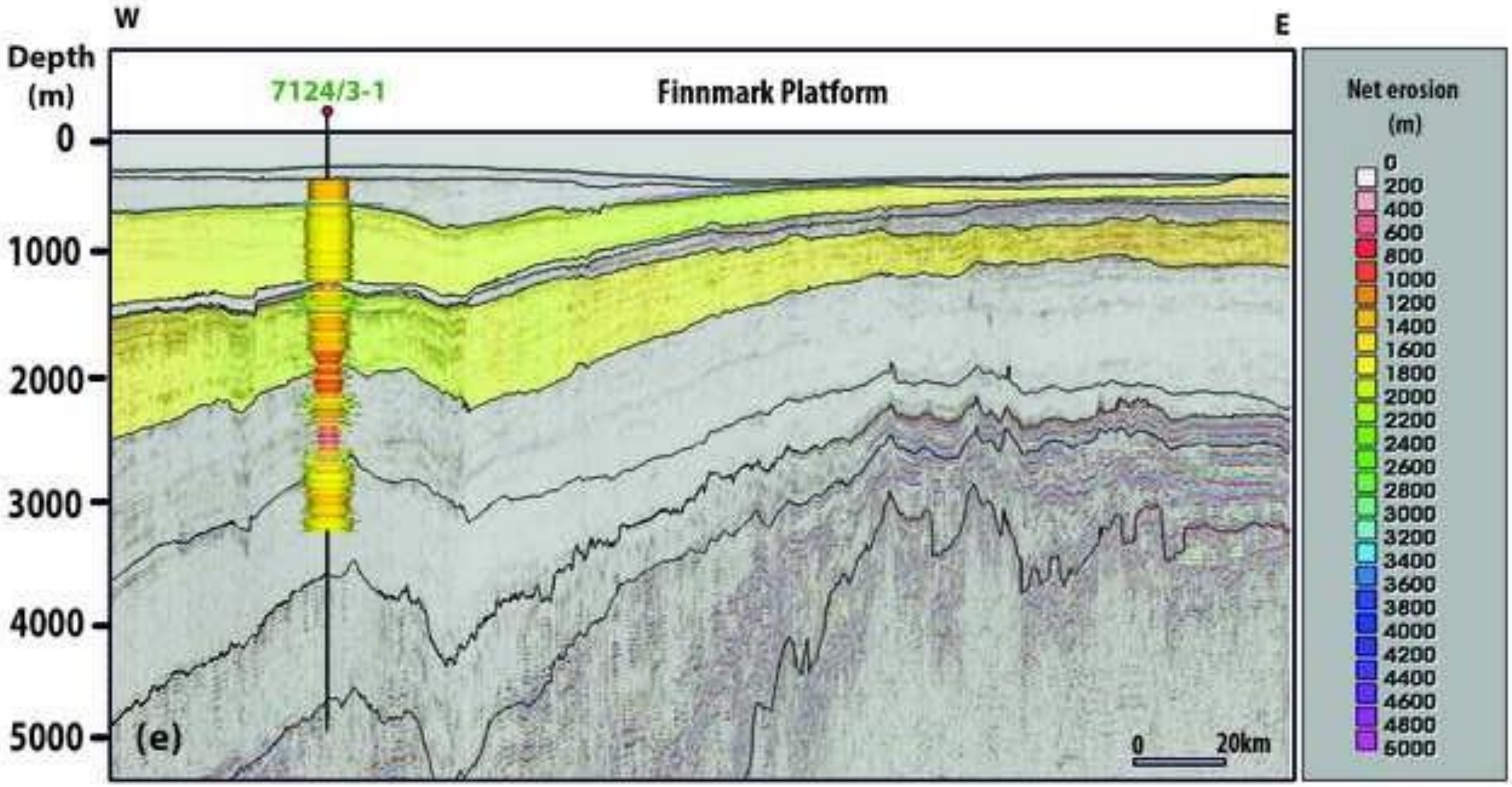

Figure 4f

Click here to access/download;figure;Figure 4f_Profile A-A_ Full_Erosion_Zoom_East.jpg

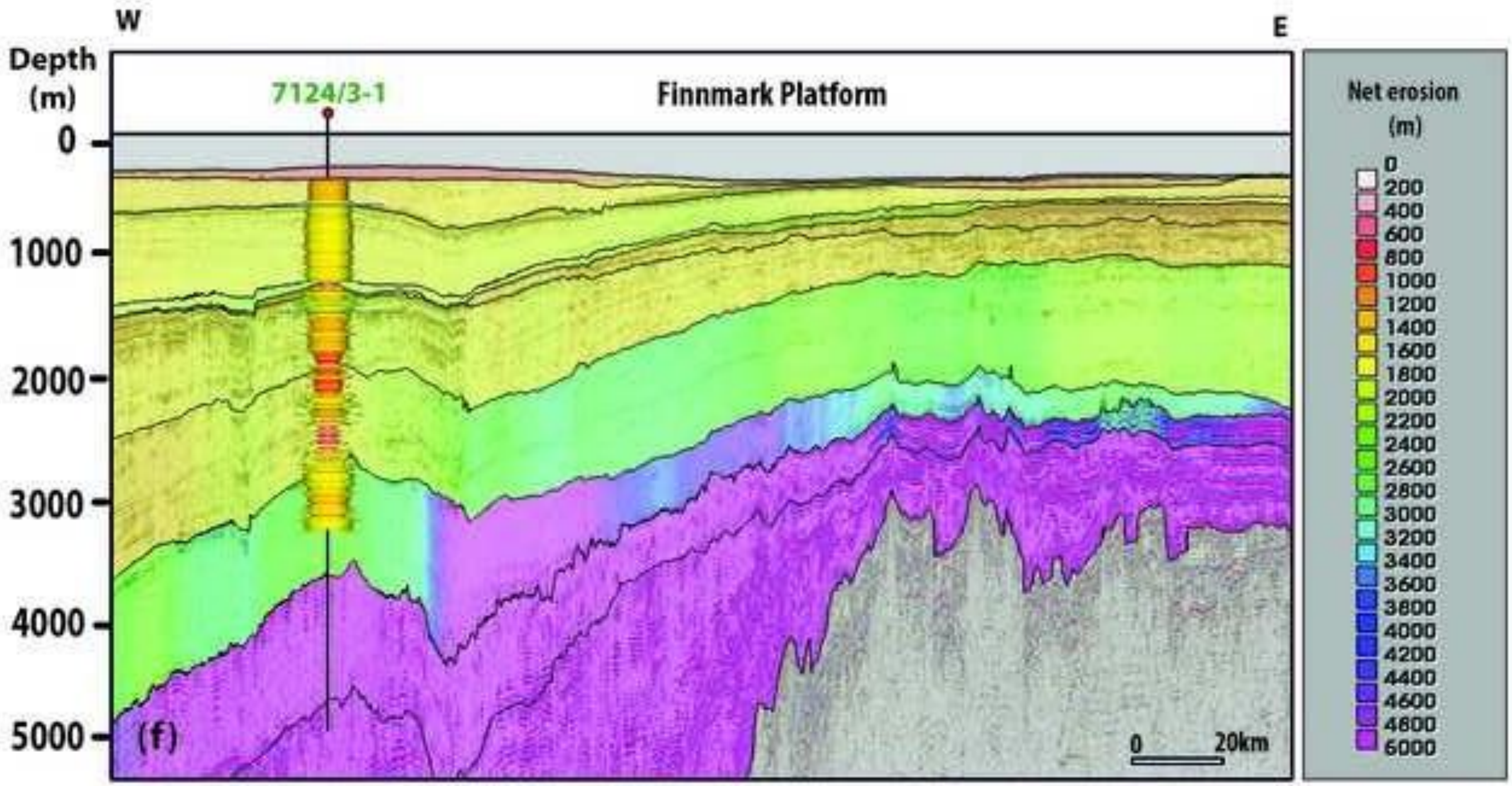

Figure 4g

Click here to access/download;figure;Figure 4g_Profile A-A_Geoseismic_Zoom_Middle.jpg

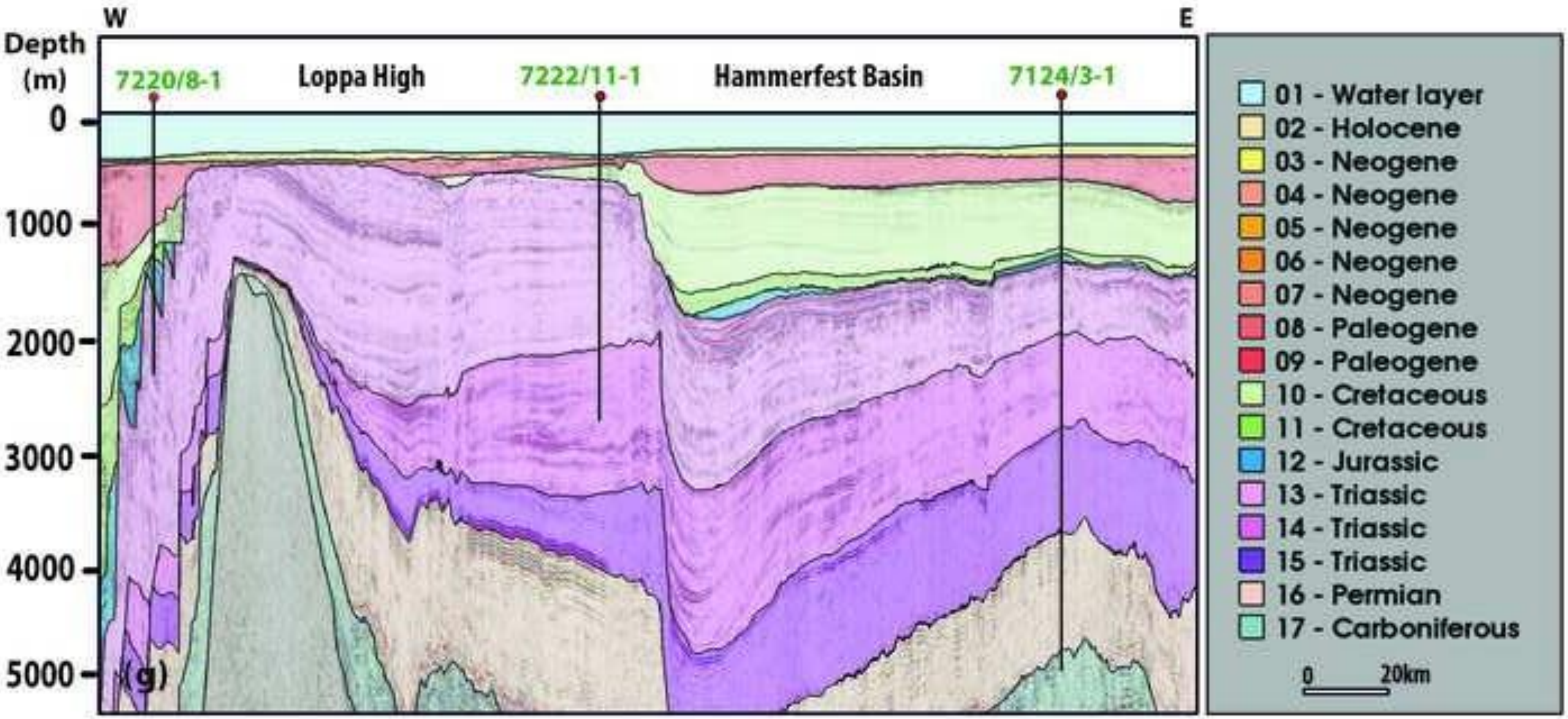

Figure 4h

Click here to access/download;figure;Figure 4h_Profile A-A_Erosion_Zoom_Middle.jpg

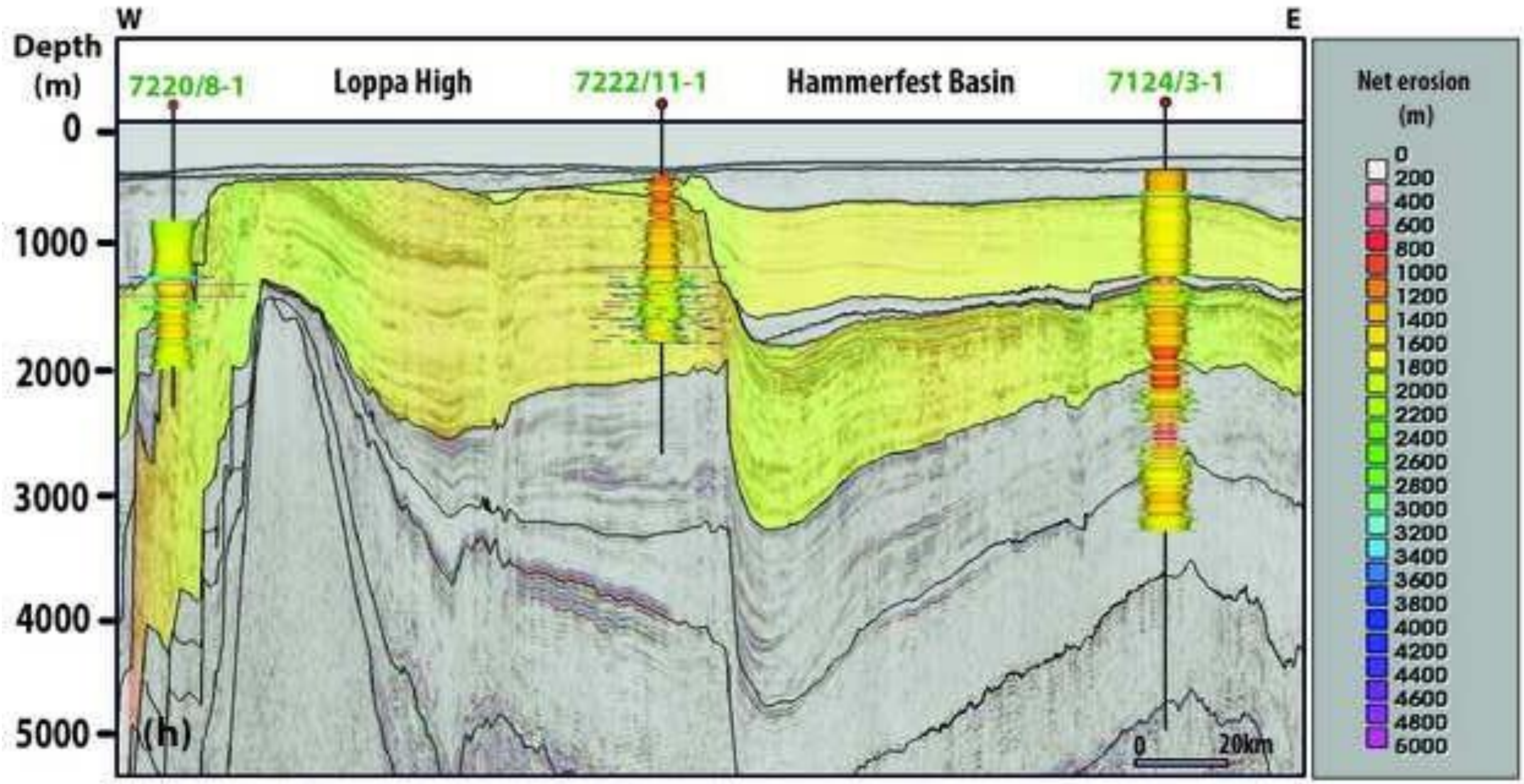

Figure 4i

Click here to access/download;figure;Figure 4i_Profile A-A_Geoseismic_Zoom_West.jpg

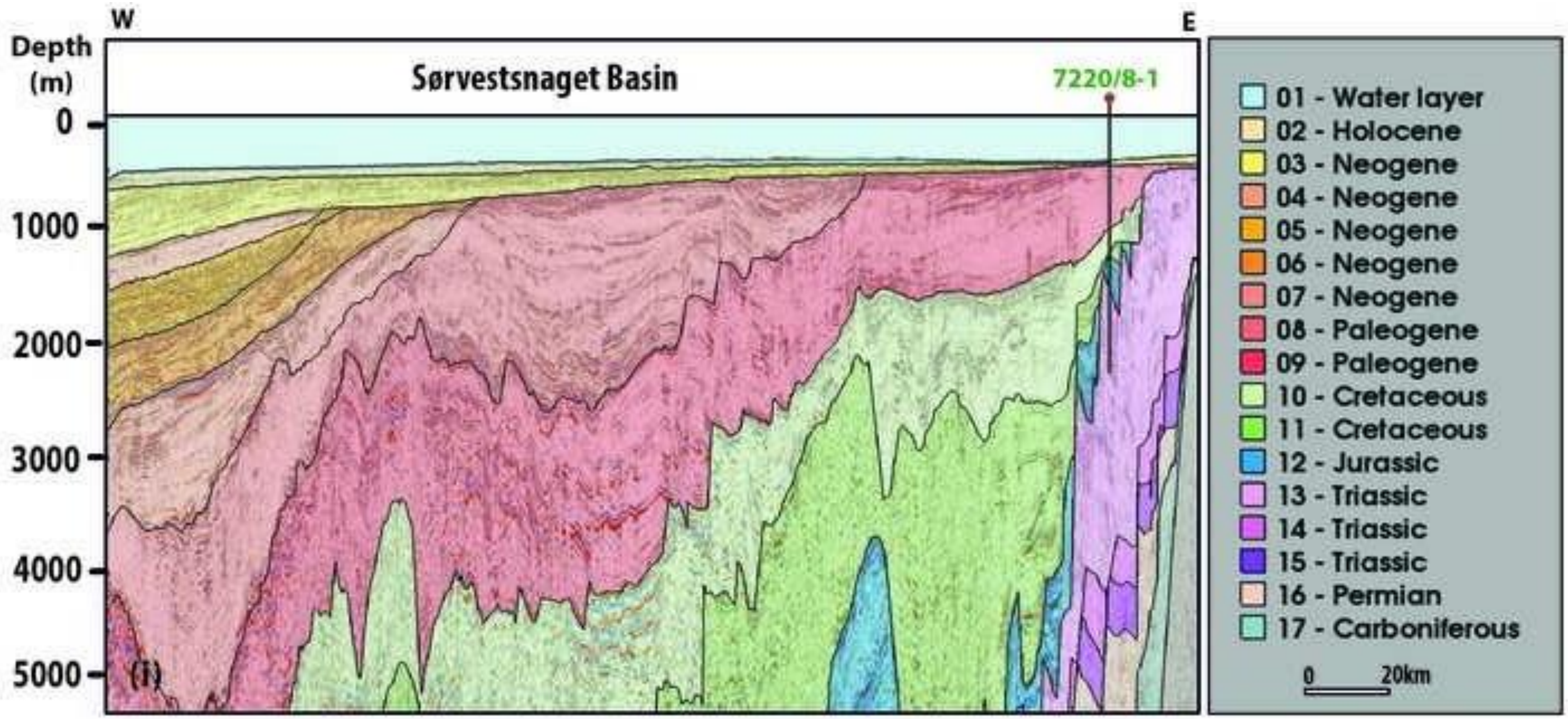

Figure 4j

Click here to access/download;figure;Figure 4j_Profile A-A_Erosion_Zoom_ West.jpg

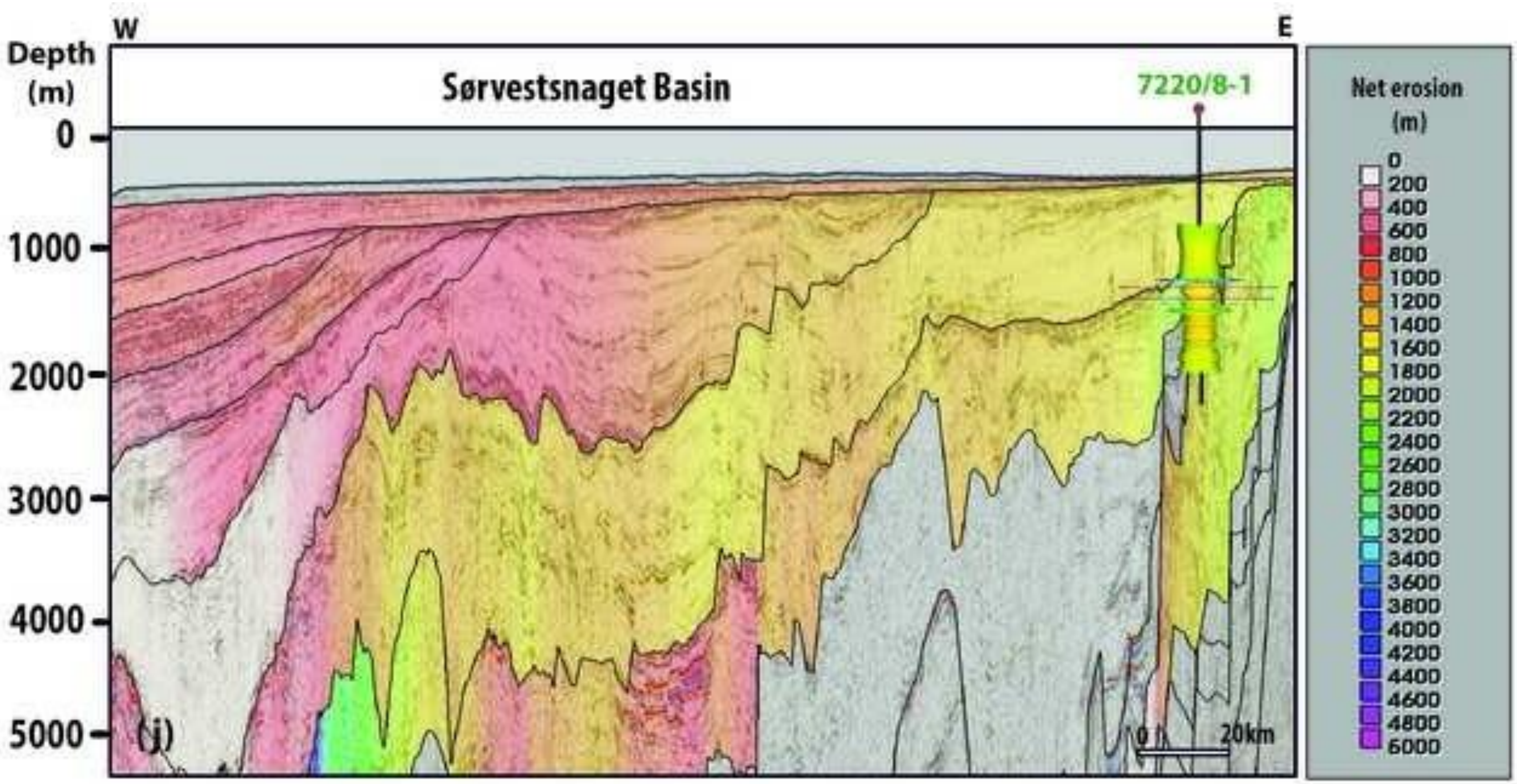

Figure 5a

Click here to access/download;figure;Figure 5a_Profile B-B_Geoseismic (2).jpg

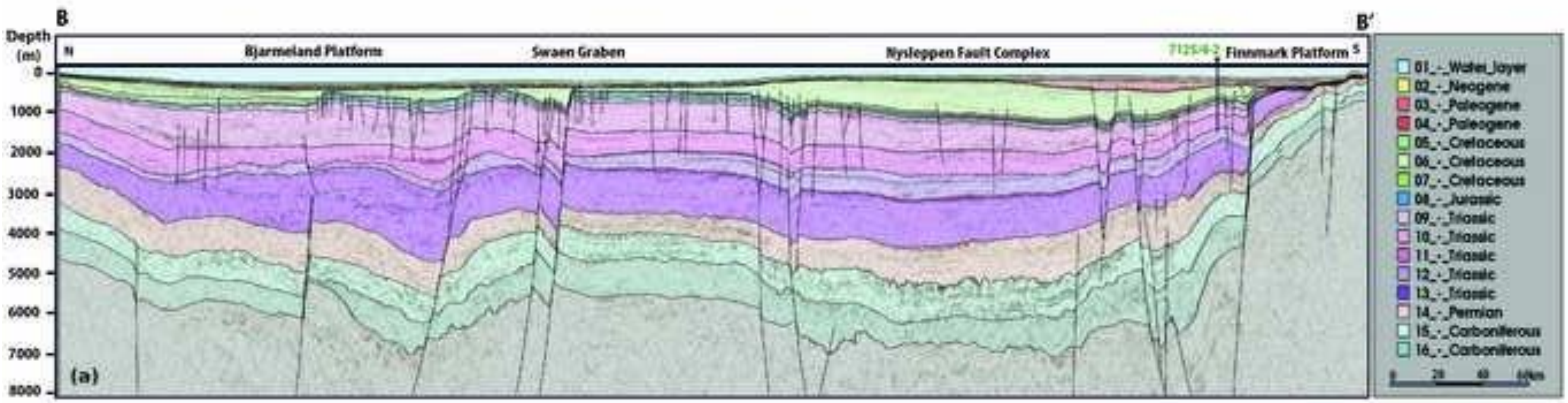

Figure 5b

Click here to access/download;figure;Figure 5b_Profile B-B_Velocity.jpg

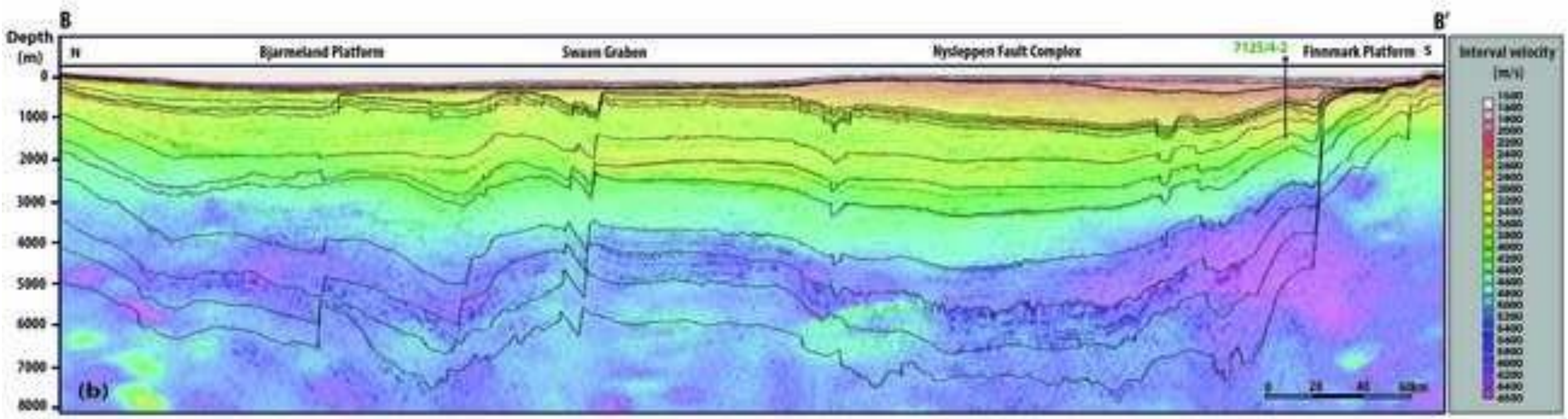

Figure 5c upper panel

Click here to access/download;figure;Figure 5c_Profile B-B_Erosion.jpg

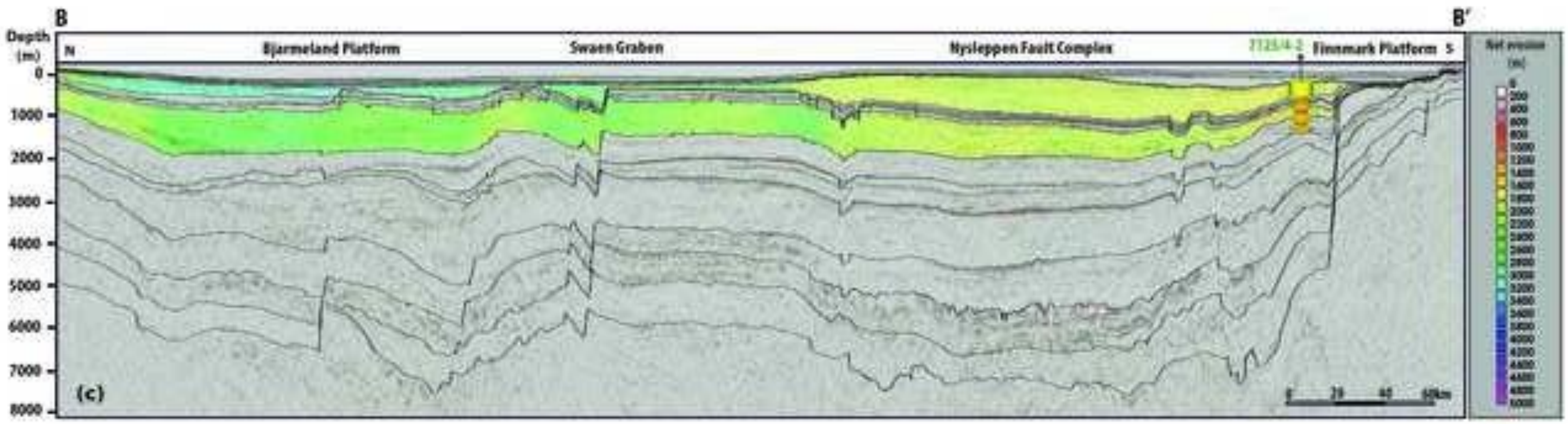

figure 5c lower panel

Click here to access/download;figure;Profile2 dataV2testSimple(1).jpg

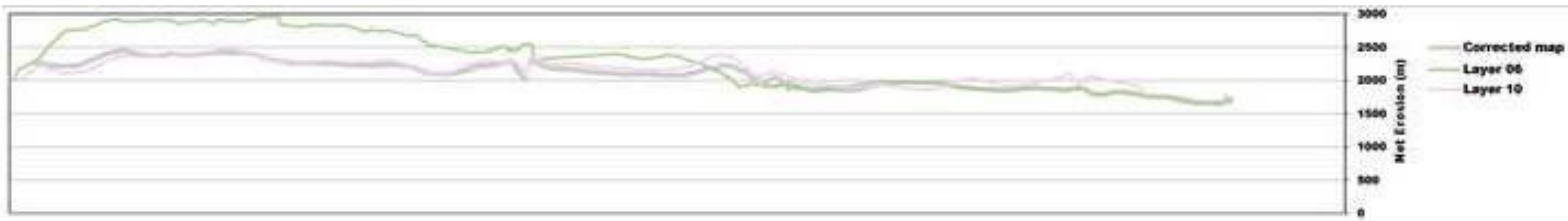

Figure 5d

Click here to access/download;figure;Figure 5d_Profile B-B_Geoseismic_Zoom_South.jpg

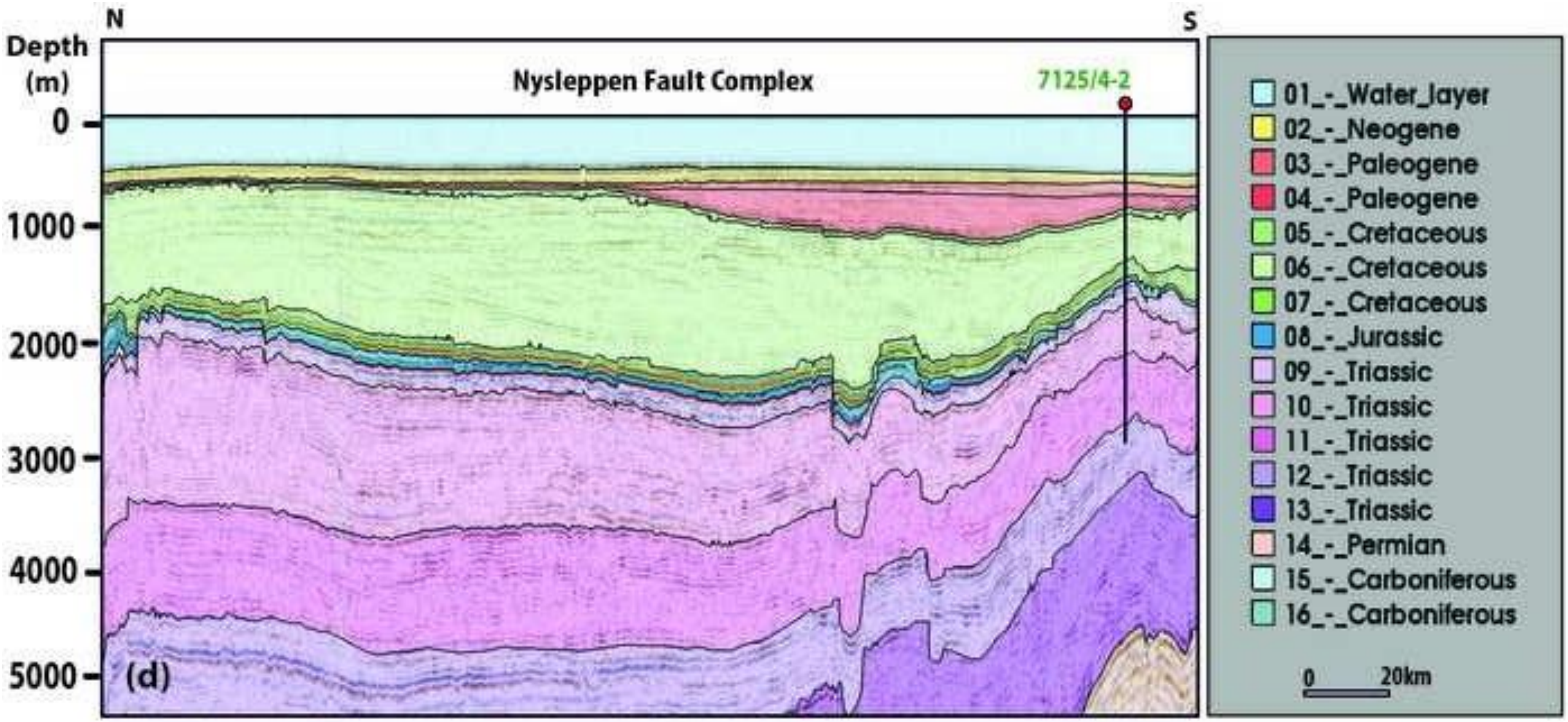

Figure 5e

Click here to access/download;figure;Figure 5e_Profile B-B_Erosion_Zoom_South.jpg

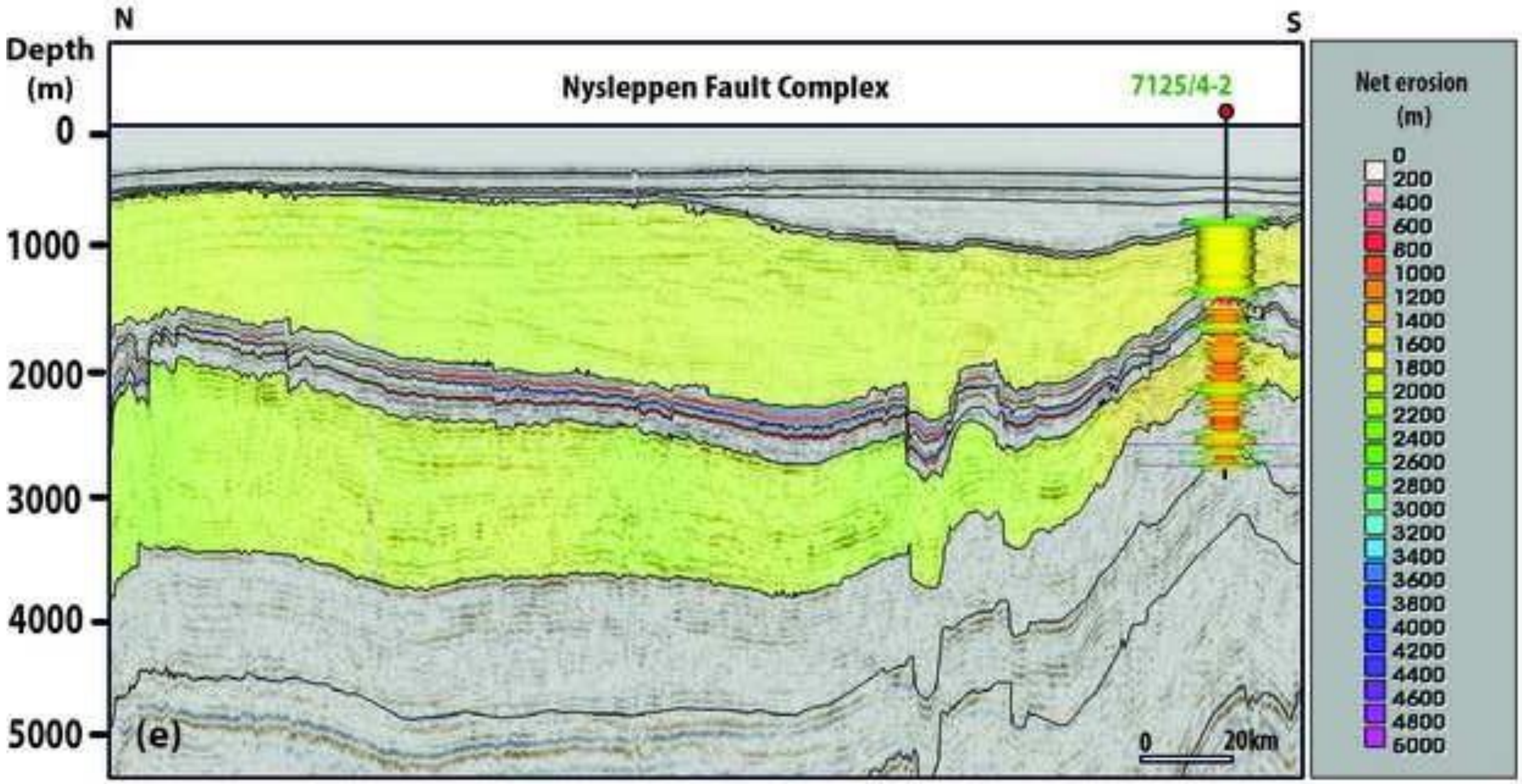

Figure 5f

Click here to access/download;figure;Figure 5f_Profile B-B_Geoseismic_Zoom_North.jpg

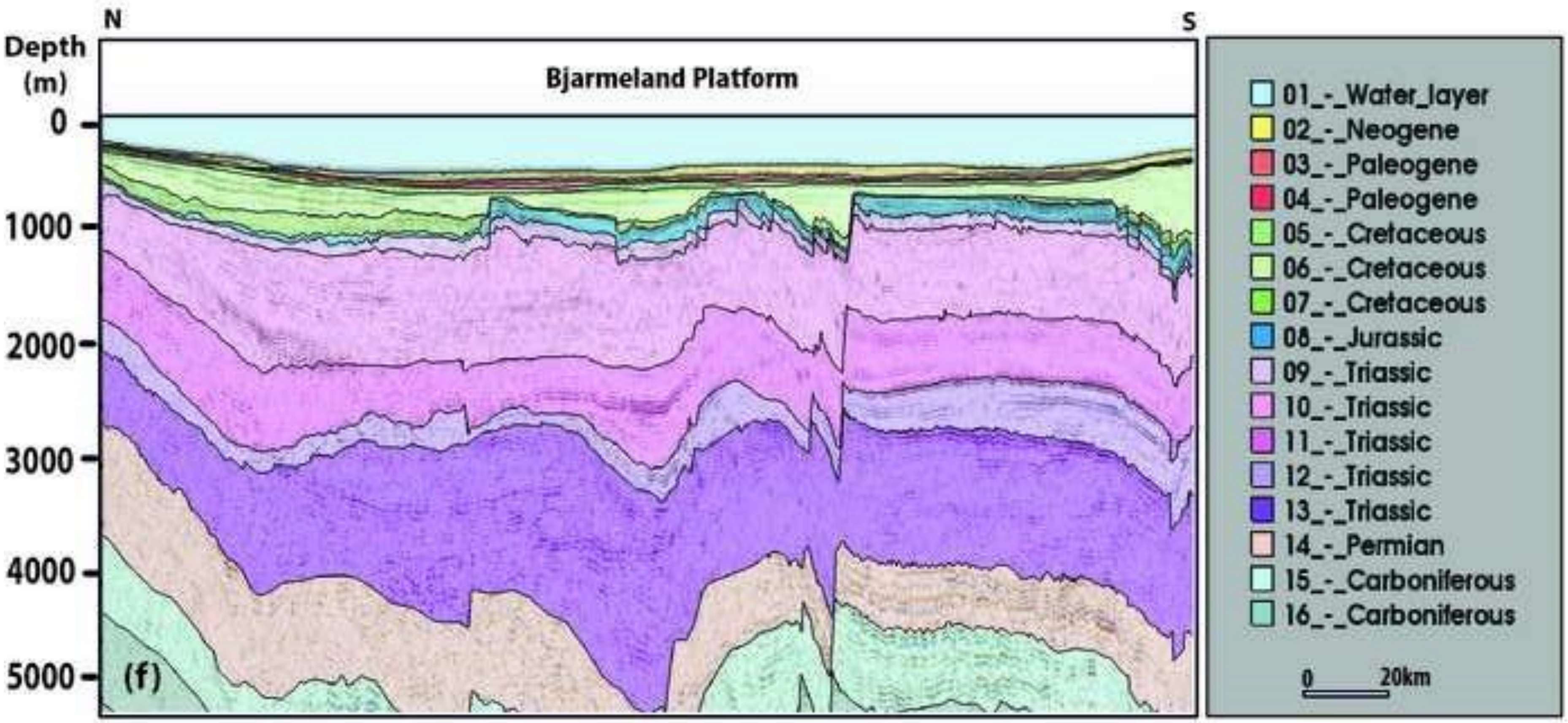

Figure 5g

Click here to access/download;figure;Figure 5g_Profile B-B_Erosion_Zoom_North.jpg

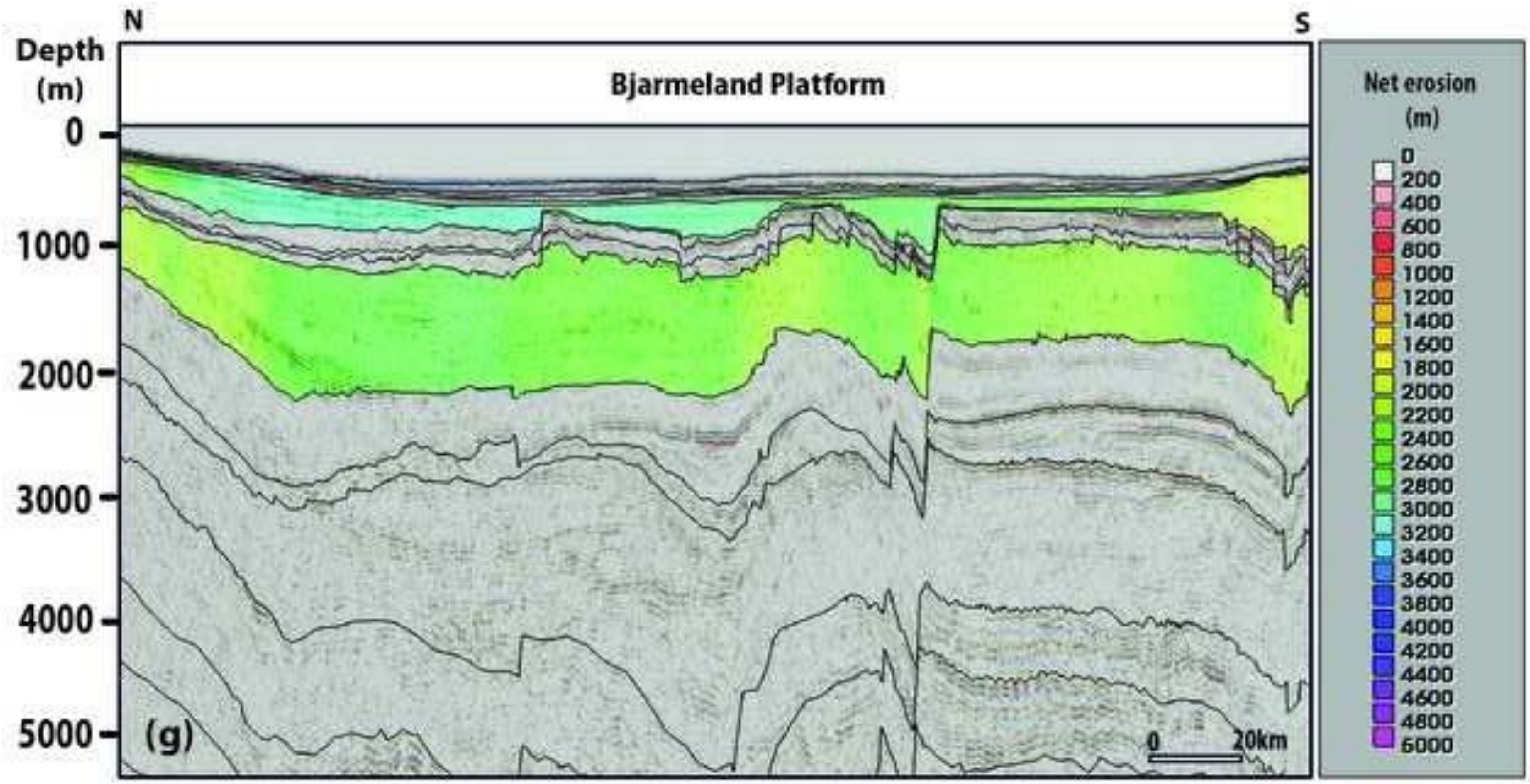

Figure 5h

Click here to access/download;figure;Figure 5h_Profile B-B_Erosion_Zoom_ North.jpg

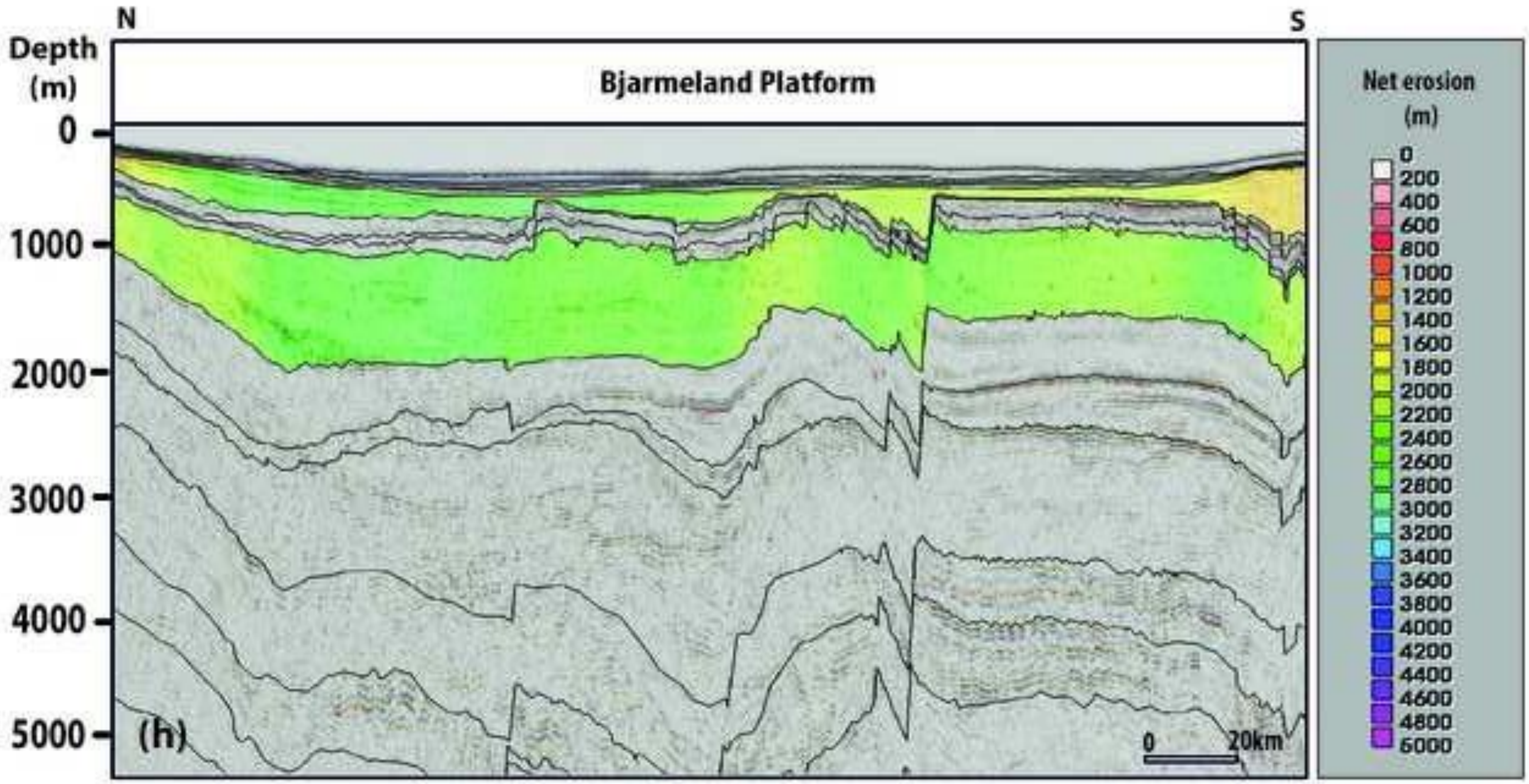

Figure 6a

Click here to access/download;figure;Figure 6a_ProfileC-C_Geoseismic.jpg

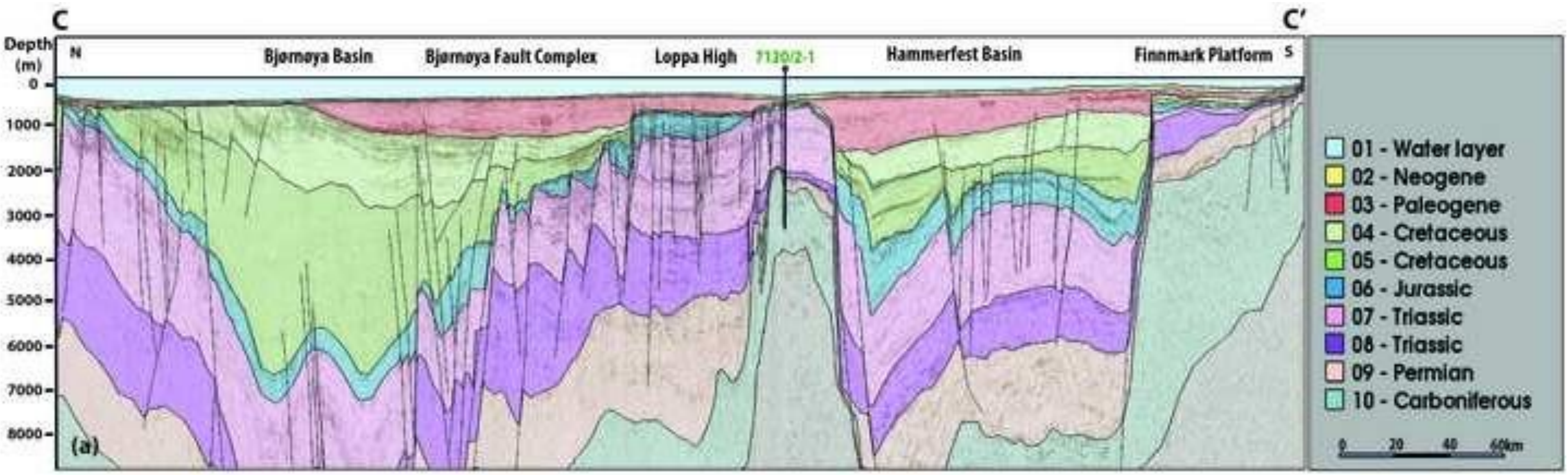

Figure 6b

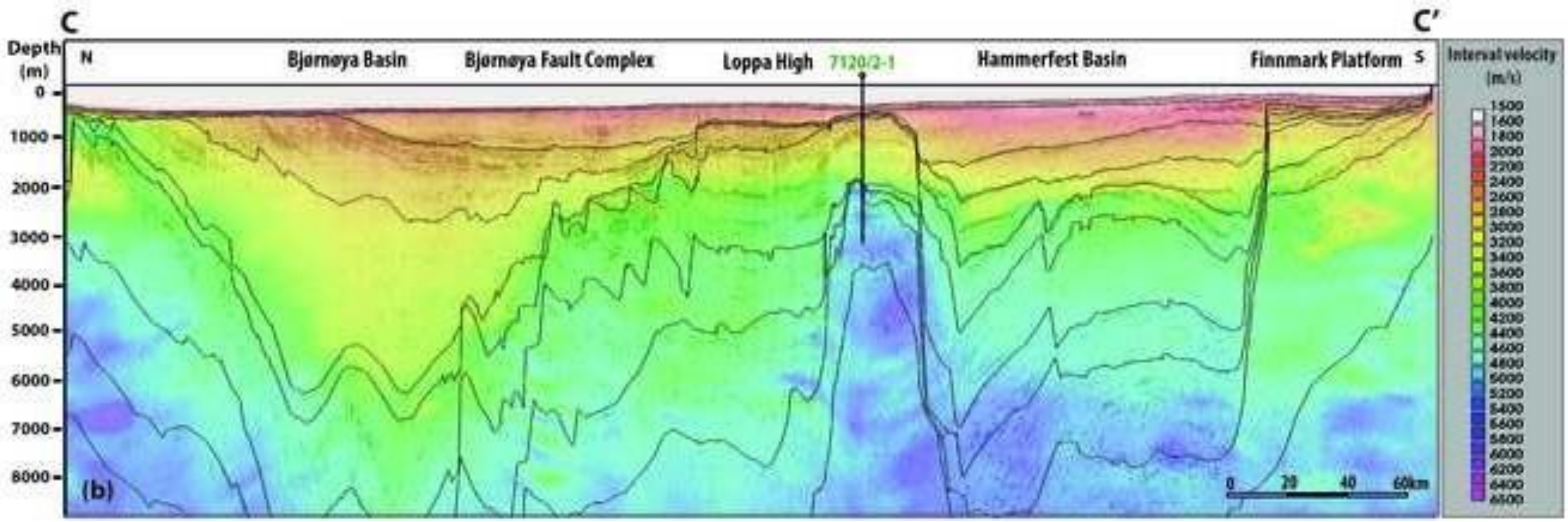
C
C'
Depth (m)
0
1000
2000
3000
4000
5000
6000
7000
8000
N
Bjørnøya Basin
Bjørnøya Fault Complex
Loppa High
7120/2-1
Hammerfest Basin
Finnmark Platform
S
(b)
0
20
40
60km
Interval velocity (m/s)
1500
1600
1800
2000
2200
2400
2600
2800
3000
3200
3400
3600
3800
4000
4200
4400
4600
4800
5000
5200
5400
5600
5800
6000
6200
6400
6500

Figure 6c upper panel

Click here to access/download;figure;Figure 6c_Profile C-C_Erosion.jpg

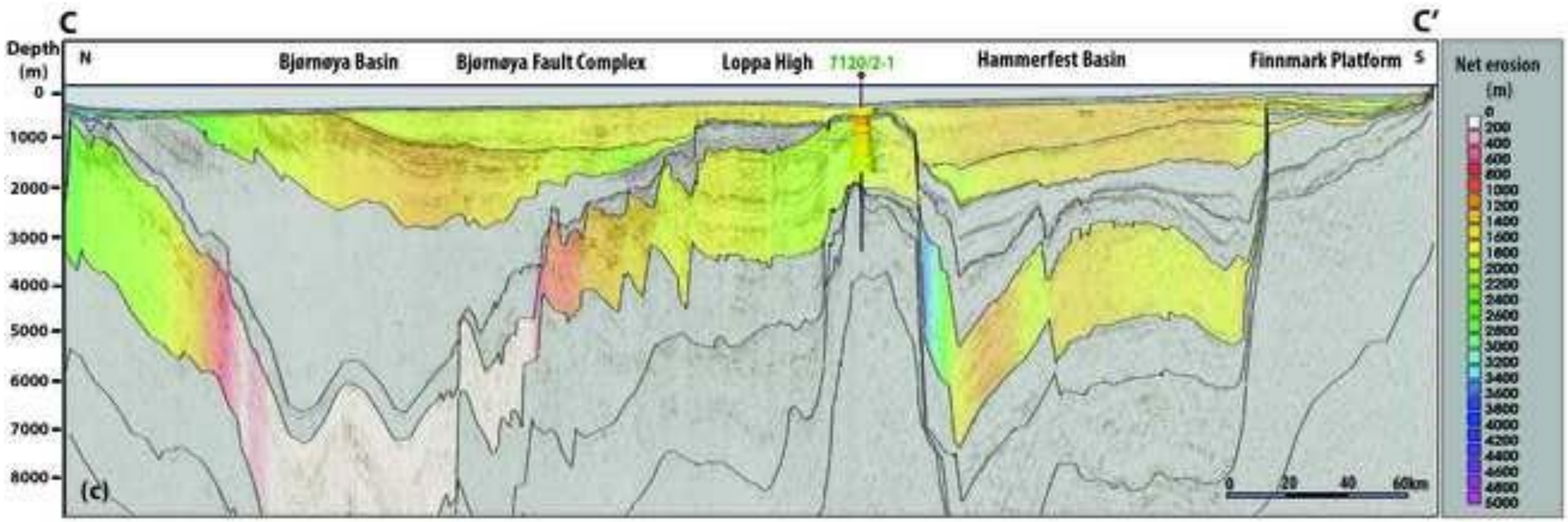

figure 6c lower panel

Click here to access/download;figure;Profile3 dataV2testSimple(1).jpg

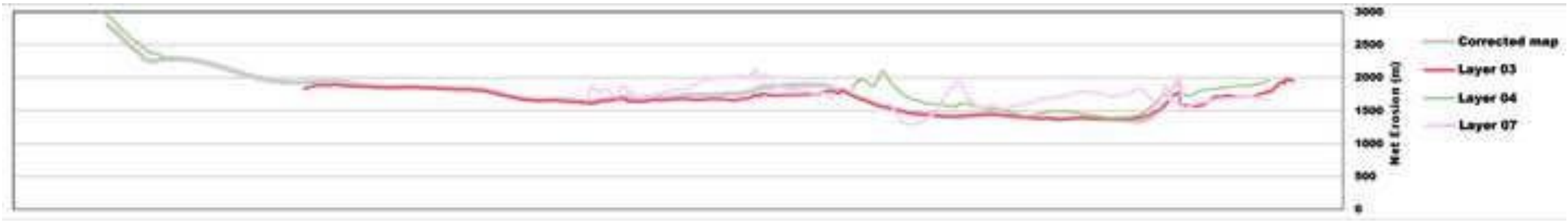

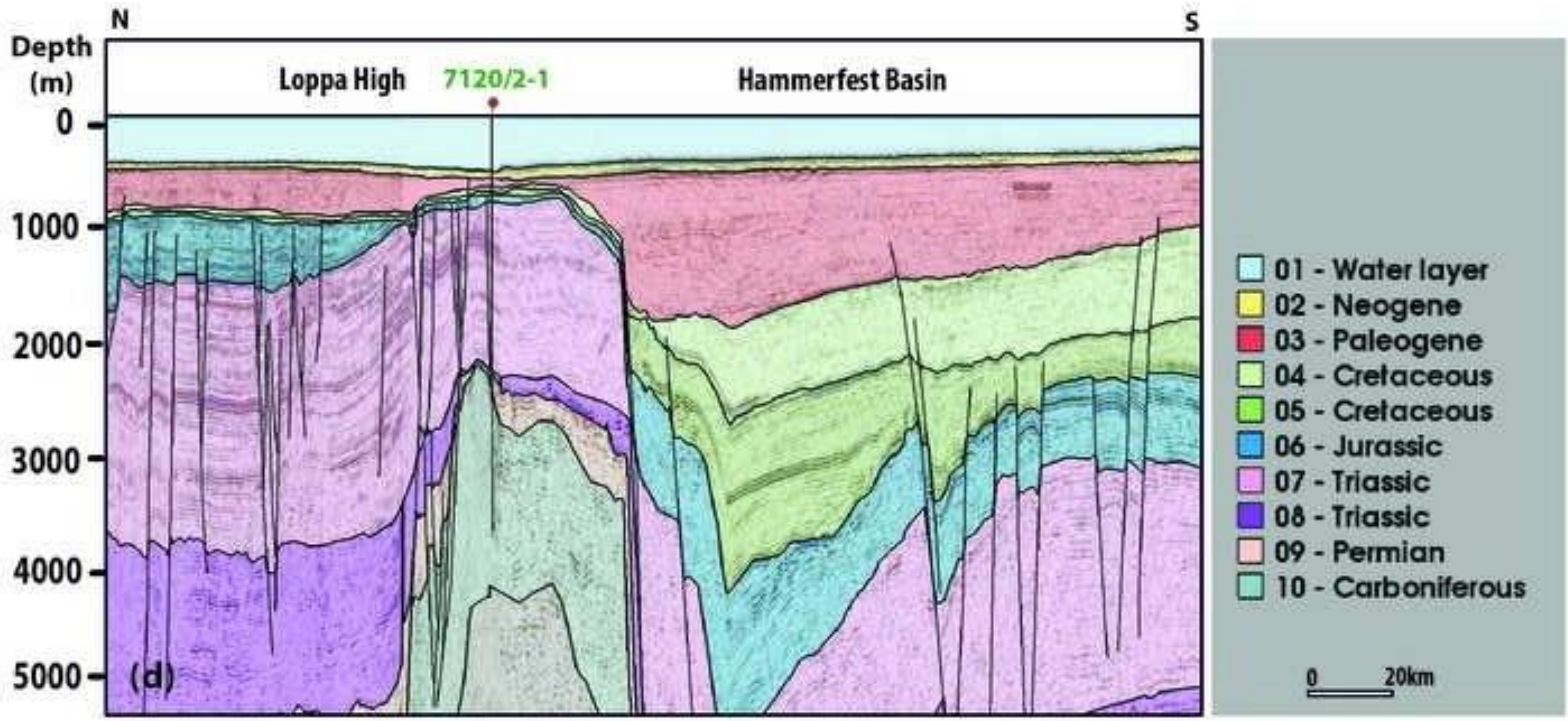
N
S
Depth (m)
0
1000
2000
3000
4000
5000
Loppa High
7120/2-1
Hammerfest Basin
(d)
01 - Water layer
02 - Neogene
03 - Paleogene
04 - Cretaceous
05 - Cretaceous
06 - Jurassic
07 - Triassic
08 - Triassic
09 - Permian
10 - Carboniferous
0
20km

figure 6e

Click here to access/download;figure;Figure 6e_Profile C-C_ZoomMiddle.jpg

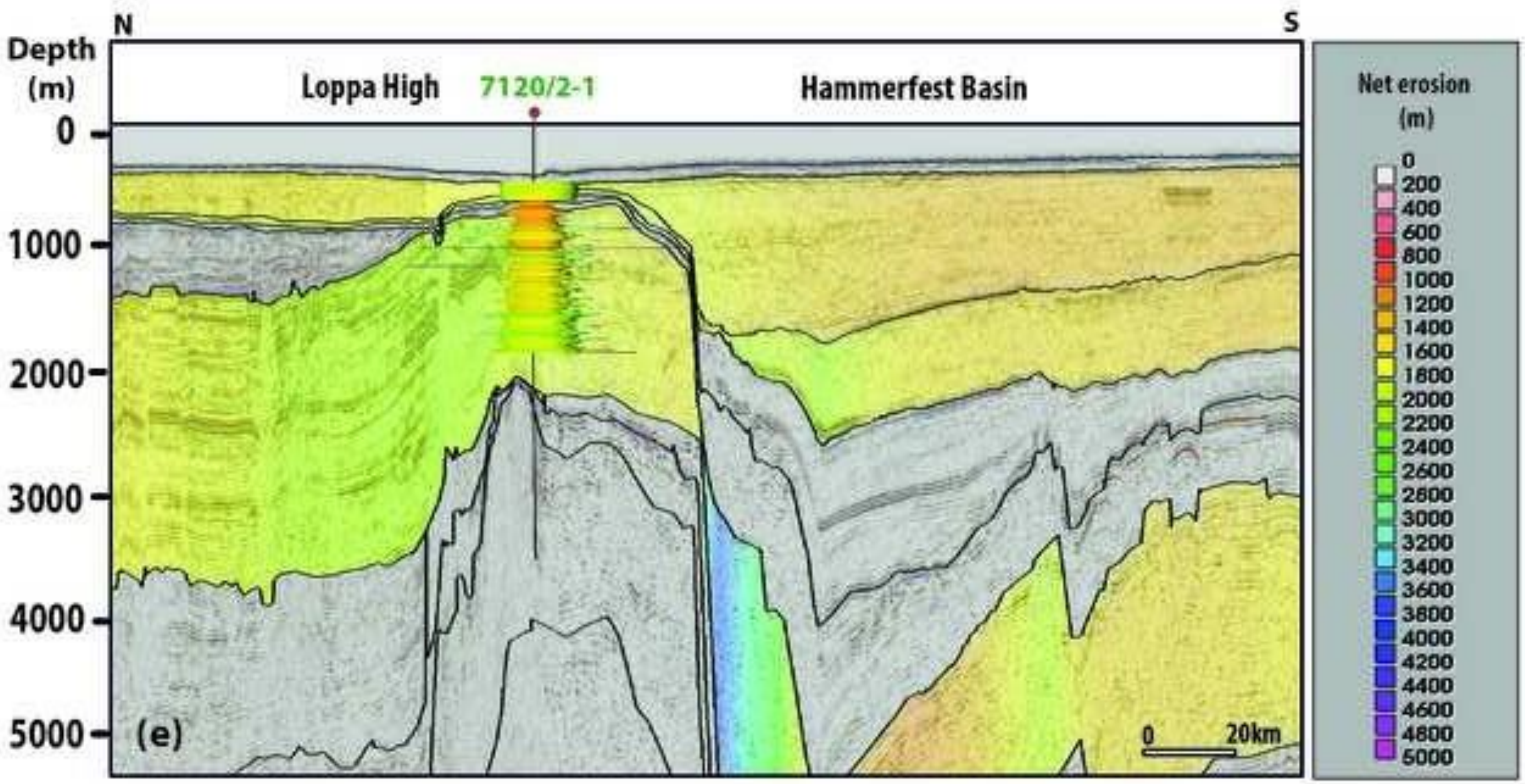

Figure 7 Click here to access/download;figure;Figure 7_Paleogene map.jpg

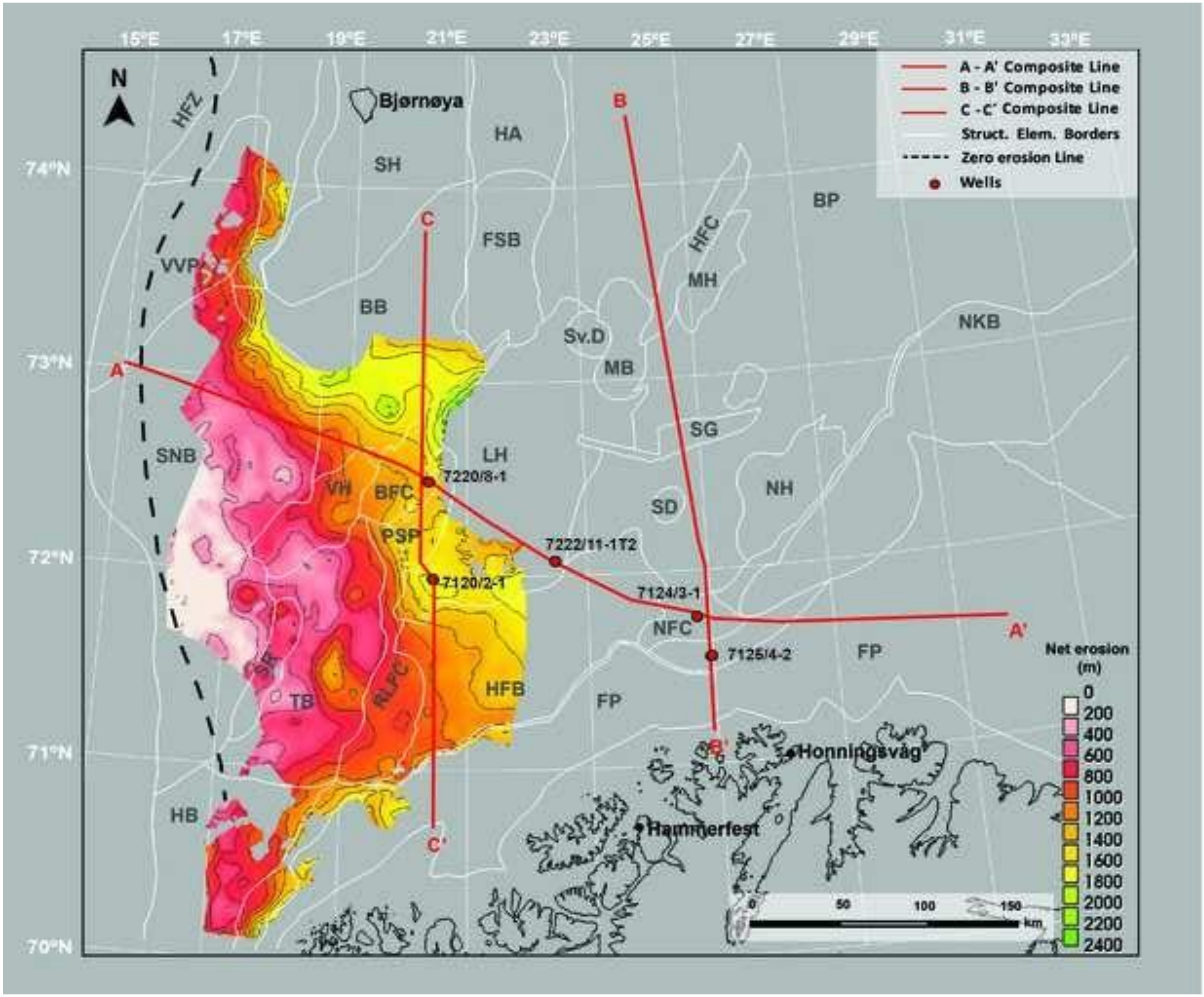

Figure 8

Click here to access/download;figure;Figure 8_Cretaceous map.jpg

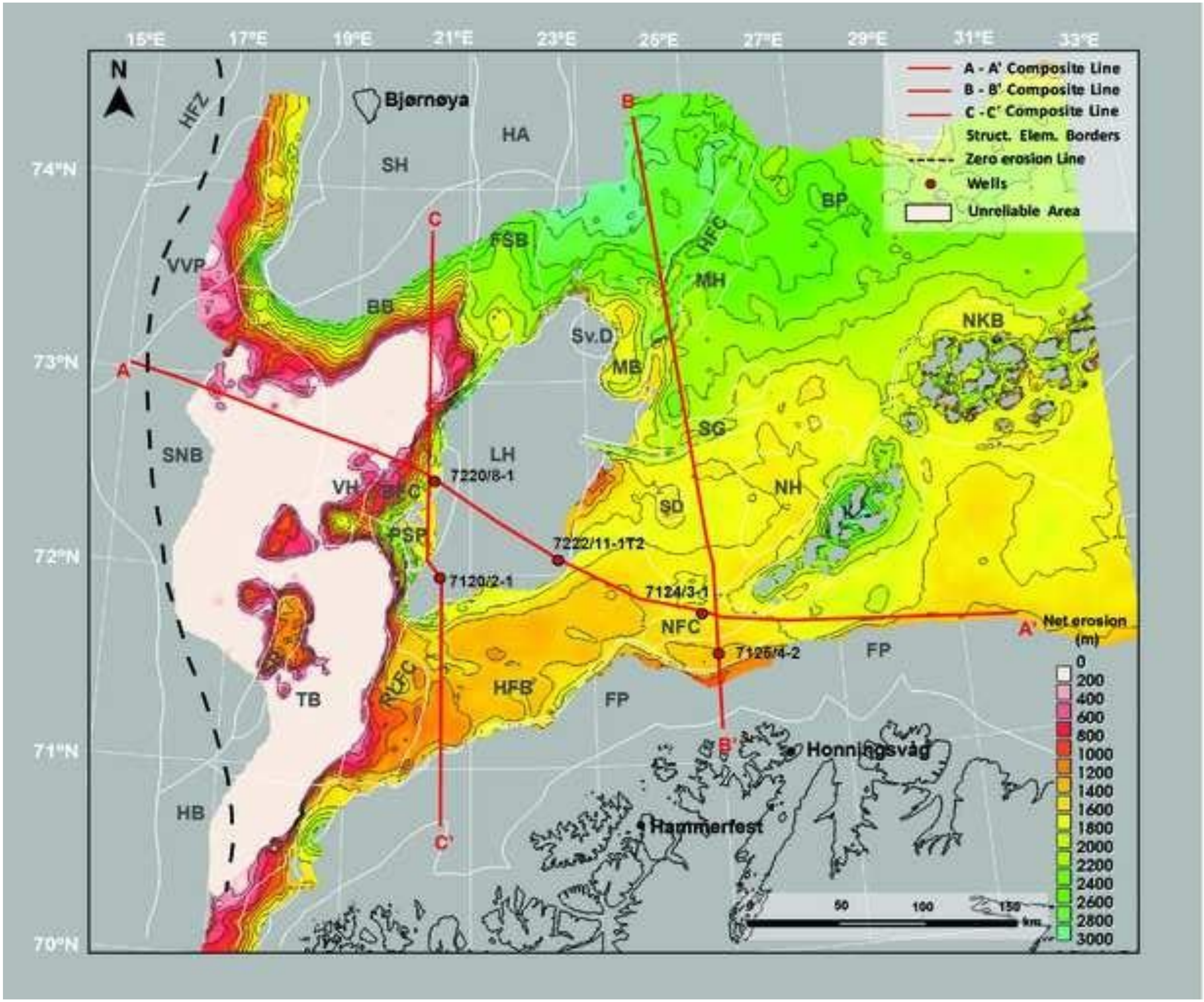

Figure 9

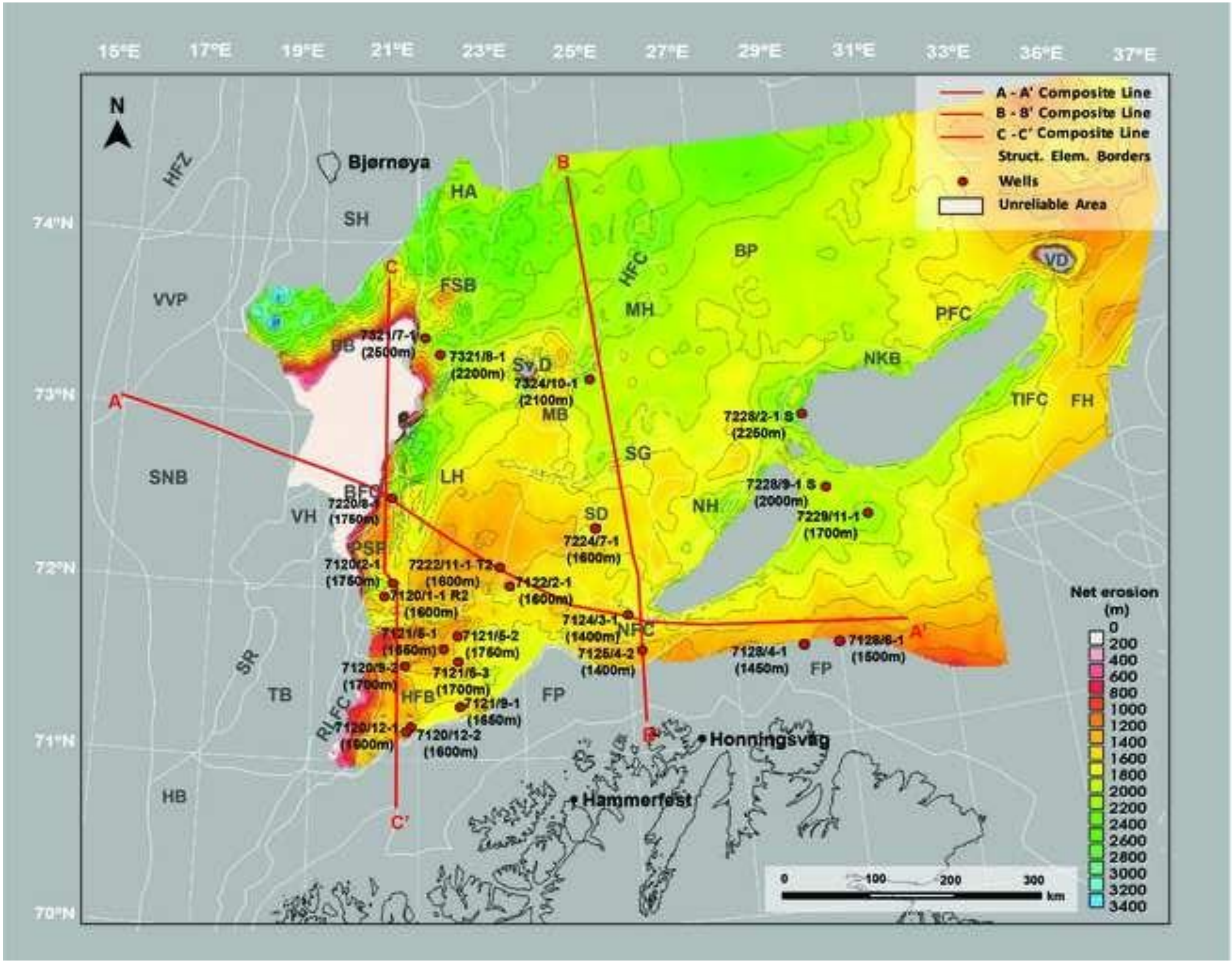

15°E
17°E
19°E
21°E
23°E
25°E
27°E
29°E
31°E
33°E
35°E
37°E
74°N
73°N
72°N
71°N
70°N
N
A - A' Composite Line
B - B' Composite Line
C - C' Composite Line
Struct. Elem. Borders
Wells
Unreliable Area
Bjørnøya
HFZ
SH
HA
VVP
FSB
BP
HFC
MH
PFC
NKB
TIFC
FH
VD
SNB
LH
MB
SG
NH
SD
VH
BFC
PSP
NFC
FP
SR
TB
HFB
RLFC
HB
Honningsvåg
Hammerfest
7321/7-1 (2500m)
7321/8-1 (2200m)
7324/10-1 (2100m)
7228/2-1 S (2250m)
7228/9-1 S (2000m)
7229/11-1 (1700m)
7220/8-1 (1750m)
7224/7-1 (1600m)
7120/2-1 (1750m)
7222/11-1 T2 (1600m)
7122/2-1 (1600m)
7120/1-1 R2 (1600m)
7124/3-1 (1400m)
7125/4-2 (1400m)
7128/4-1 (1450m)
7128/6-1 (1500m)
7121/5-1 (1650m)
7121/5-2 (1750m)
7120/9-2 (1700m)
7121/5-3 (1700m)
7121/9-1 (1650m)
7120/12-1 (1600m)
7120/12-2 (1600m)
0
100
200
300
km
Net erosion (m)
0
200
400
600
800
1000
1200
1400
1600
1800
2000
2200
2400
2600
2800
3000
3200
3400

figure 10

Click here to access/download;figure;Figure_10.jpg

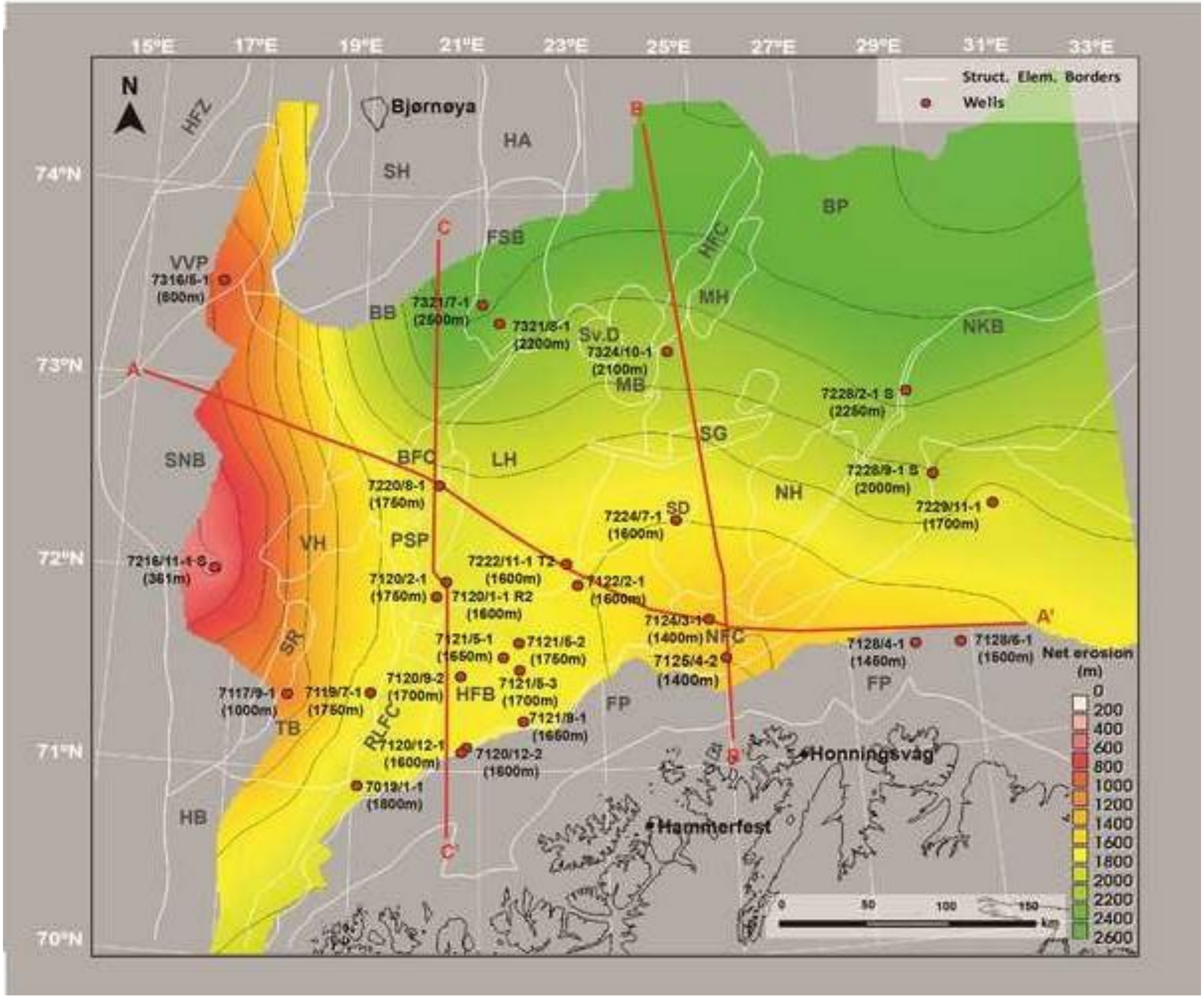

Figure 11 Click here to access/download;figure;Figure 11_Crossplot.jpg

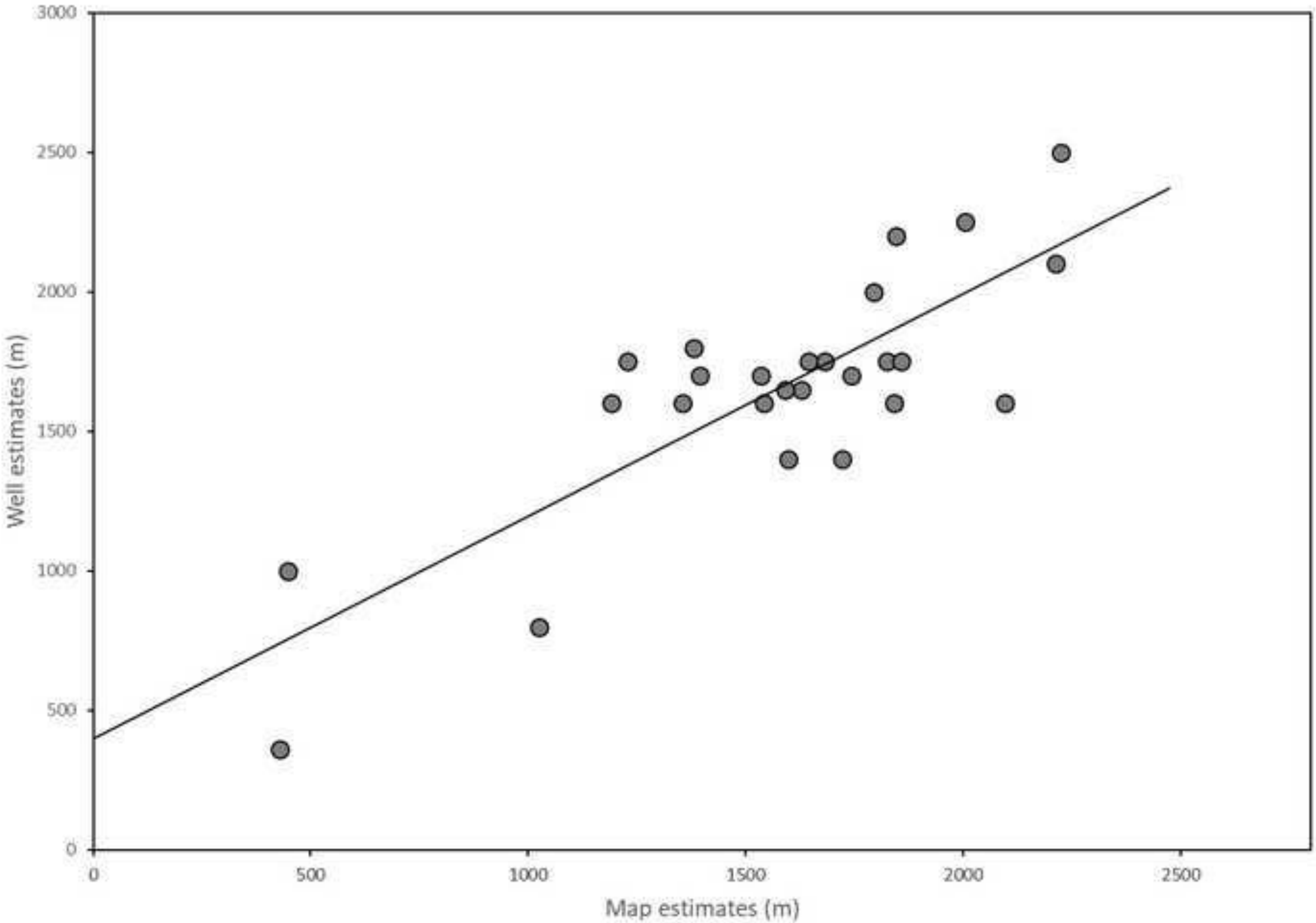

figure 12 Click here to access/download;figure;Figure_12.jpg